Chemistry Research and Applications

Hongshun Yang
Editor

Atomic Force Microscopy (AFM)

Principles, Modes of Operation and Limitations

NOVA

ATOMIC FORCE MICROSCOPY (AFM)

PRINCIPLES, MODES OF OPERATION AND LIMITATIONS

CHEMISTRY RESEARCH AND APPLICATION

ATOMIC FORCE MICROSCOPY (AFM)

PRINCIPLES, MODES OF OPERATION AND LIMITATIONS

HONGSHUN YANG, PH.D.
EDITOR

nova publishers
New York

CONTENTS

In: Atomic Force Microscopy (AFM)
Editor: Hongshun Yang
ISBN: 978-1-63117-172-7

Chapter 1

APPLICATION OF ATOMIC FORCE MICROSCOPY IN FOOD-RELATED MACROMOLECULES

Xiao Feng[1,2], Shaojuan Lai[3], Meng Li[4], Caili Fu[1,2], Fusheng Chen[4] and Hongshun Yang[1,2*]

[1]Food Science and Technology Programme,
Department of Chemistry, National University of Singapore, Singapore, Singapore
[2]National University of Singapore (Suzhou) Research Institute,
Suzhou, Jiangsu, P.R. China
[3]College of Biological Engineering, Henan University of Technology,
Zhengzhou, Henan, China
[4]College of Food Science and Technology, Henan University
of Technology, Zhengzhou, Henan, China

ABSTRACT

Microscopy methodology has advantages over many other characterization techniques in that it can directly visualize the heterogeneity of samples. However, at molecular or nanoscale level, some microscopies can not provide images of enough resolution when images' sizes are small. Microscopic analysis at the single molecule level can be achieved by scanning probe methods including atomic force microscopy (AFM). AFM is able to image almost any type of surface, including polymers, ceramics, composites, glasses, and biological samples. It requires neither a vacuum environment nor any special sample preparation. In addition, it can be used in either an ambient or liquid environment. In this review, the structures of chitosan, pectin, biomass, casein and living cells surface were reviewed using AFM. Applications of AFM in the study on the mucoadhesion mechanism of pectin, interactions of Galectin 3 and β-galactobiose, as

* Corresponding author: Hongshun Yang. Food Science and Technology Programme, Department of Chemistry, National University of Singapore, 3 Science Drive 3, Singapore 117543, Singapore. National University of Singapore (Suzhou) Research Institute, 377 Lin Quan Street, Suzhou Industrial Park, Suzhou, Jiangsu 215123, P.R. China. Tel: +65-65164695, Fax: +65-67757895. E-mail address: chmynghs@nus.edu.sg, hongshunyang @hotmail.com.

well as fractal properties of macrophage membrane were introduced. The relationship of apple texture with cell wall nanostructure techniques was also illustrated.

Keywords: Atomic force microscopy (AFM); Food Science; Nanotechnology; Polysaccharides; Pectin

1. AFM Overview

Microscopy methodology can directly visualize the heterogeneity of samples and hence this methodology is broadly used to investigate different structures with benefits over many other characterization techniques. Using light and electron microscopy, numerous cell structures have been analyzed over the years. The invention of atomic force microscope (AFM) made possible to analyze biological samples at the nanoscale without the restriction of other microscopy methods such as the transmission electron microscopy and scanning tunneling microscope [1]. AFM can work without vacuum conditions and doesn't require the need of conductivity of samples. In addition, AFM offers a very high resolution in the vertical z axis and thus living cells can be analyzed at the nanoscale spatial resolution.

AFM is the image-based microscopy method measuring the samples in three dimensions, x, y, and z (normal to the sample surface). It was first invented in 1986 by Binnig with the aim of overcoming the limitations of other microscopy method and was introduced to the field of biological sciences by Hansma [2, 3]. AFM images are obtained through measuring the changes in the magnitude of interactions between AFM probe and the surface samples when the atomically sharp probe scans the surface. Figure 1a shows a typical atomic force microscope constituting of a piezoelectric scanner, cantilever with a sharp probe, laser, photodiode detector, and feedback electronics. There are two kinds of sample-placing methods [4]. When the sample sits on the piezoelectric scanner (e.g., Figure 1A), the cantilever keeps a fixed position. This is the major method used in many commercial microscope systems. In other methods, the sample is kept stationary and the AFM cantilever keeps moving while the piezoelectric scanner is attached to the AFM cantilever holder.

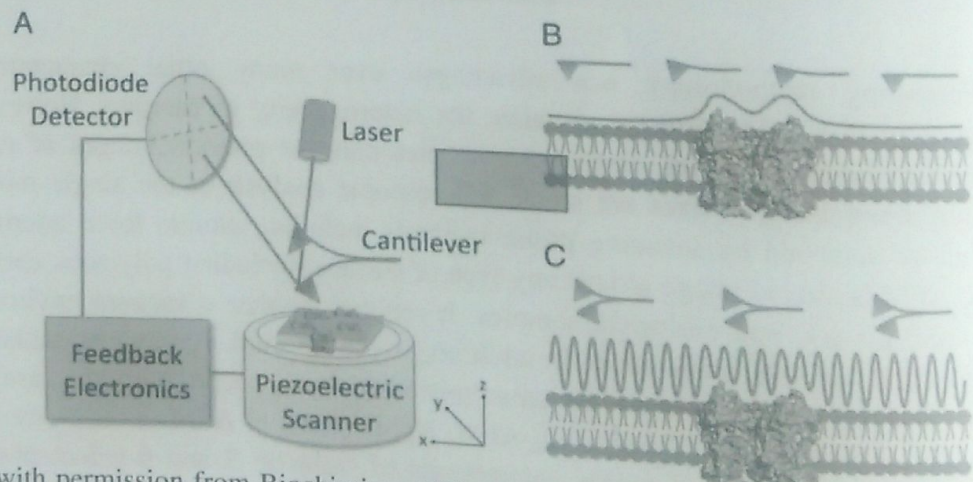

Reprinted with permission from Biochimica et Biophysica Acta 2014, 1838, 56-68. Copyright (2014). Elsevier, Inc. [4].

Figure 1. AFM overview. (A) Components of an atomic force microscope. (B) Contact mode imaging. (C) Tapping mode or intermittent contact mode imaging.

AFM scanning can be operated in two main modes: contact mode and tapping or intermittent contact mode. In contact mode (Figure 1B), the AFM probe constantly contacts with the sample surface during the whole scanning. The deflection of the cantilever is monitored while the feedback electronics maintain constant force on the sample by adjusting the vertical position of the piezoelectric scanner.

The lateral shear forces can present in contact mode imaging while softer or loosely adsorbed samples can be damaged or deformed by interactive forces between sample and the AFM tip Alternatively, tapping mode is more suitable for this type of samples. In tapping mode (Figure 1C), the cantilever is oscillated and the oscillation amplitude is monitored to change when the height of the sample changes. The feedback electronics keep a constant applied force by adjusting the vertical position of the piezoelectric scanner.

AFM is a convincing tool to analyze different structures and function of biomolecules [5-6]. Figure 2 shows single molecule force spectroscopy for structures and function analysis with AFM [7]. One of the key functionalization strategies is to minimize the non-specific forces and isolate the relevant interaction (Figure 2). It can be performed to minimize non-specific interactions by connecting the simplest attachment with the molecule to the tip with a short rigid linker.

The rest of the probe surface is often filled with a spacer (Figure 2c, I). In a physicist's view, a secondary minimum on the potential energy surface can appear when the scanner shifts the cantilever away from the surface (Figure 2d and e). To distinguish the interaction from background noise and nonspecific forces is an important function for every force spectroscopy experiment. High-resolution imaging can be performed to resolve single molecules with high-resolution AFM due to the high signal-to-noise ratio [8].

Some cellular structures and processes can be obtained with the help of the combination of optical and atomic force microscopy [9, 10]. With AFM especially a hybrid atomic force microscopy, cellular morphologies and events can be powerfully investigated. However, in order to visualize structural changes during cellular events, high-speed AFM units equipped with an optical/fluorescence detection device have been a long-standing aspiration because the conventional hybrid AFM system has the disadvantages of the slow data acquisition rates [11].

Figure 3 shows a recent novel instrument aiming to obtain high-speed AFM images of morphological changes in individual cells. Using this instrument with a developing a tip-scanning system, instead of a sample-scanning system, the time resolution will be improved, which makes it possible to image dynamic cellular events of living HeLa and 3T3 fibroblast cell.

Atomic force microscopy requires neither a vacuum environment nor any special sample preparation and can image almost any type of surface, including glasses, composites, ceramics, polymers, and biological samples in either an ambient or liquid environment [12].

Table 1 shows a comparison between AFM and other microscopes with regard to their advantages and disadvantages [1].

In this review, the structures of chitosan, pectin, biomass, casein and living cells surface using AFM were reviewed.

Applications of AFM in the mucoadhesion mechanism of pectin, interactions of Galectin 3 and β-galactobiose, as well as fractal properties of macrophage membrane were introduced. The relationship of apple texture with cell wall nanostructure techniques was also illustrated.

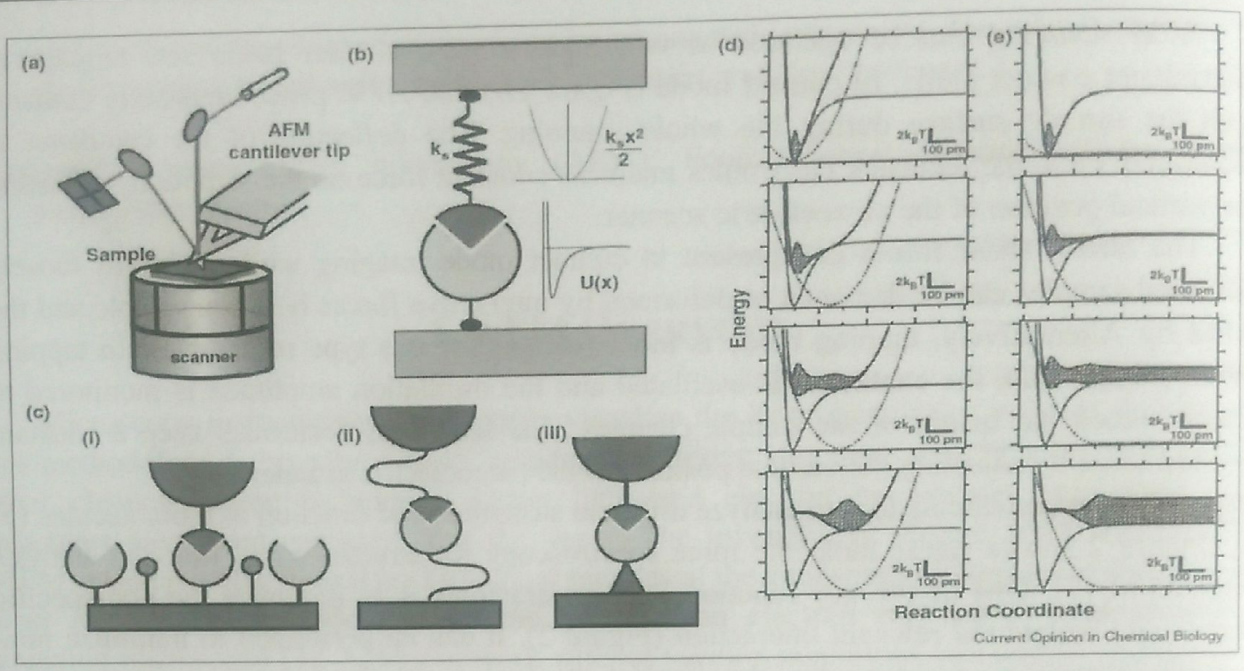

Reprinted with permission from Current opinion in chemical biology 2011, 15, 710-718. Copyright (2011), Elsevier, Inc. [7].

Figure 2. Single molecule force spectroscopy with AFM. (a) Schematics of an atomic force microscope. (b) A simplified diagram of the mechanical elements that contribute to the potential energy surface of the SMFS experiment showing the chemical bond and a loading spring. Insets show the potentials of the bond and the spring. (c) Basic strategies for probe and sample configurations that help to isolate the interaction of interest: (I) dilution; (II) tethermediated attachments; (III) sample engineering to limit the contact area. (d) and (e) Potential energy surfaces for a typical force spectroscopy experiment. An interaction potential represented by the thin solid line loaded by a harmonic spring potential (dashed line). The overall potential energy profile of the system is shown by the thick solid line. The shaded area corresponds to the Boltzmann equilibrium density of states for that potential energy profile. The graphs represent potential energy surface snapshots during loading with (d) harmonic potential, and (e) semiharmonic potential (simulations by R.W. Friddle, 2007). The interaction potential used for these simulation was represented by a Morse potential

$$U(x) = U_o\left[1 = \exp\left(-2b\left(\frac{x}{x_o} - 1\right)\right)\right]^2 \text{ with } U_o = 10{\cdot}k_BT,\ x_o = 1\,\text{Å} \text{ and } b = 1.0.$$

Table 1. Advantages and disadvantages of different microscopy techniques

Characteristics	Microscopy				
	AFM	LM	SEM	TEM	CLSM
Advantages	High resolution, nanoscale Minimal sample preparation, near native status 2D and 3D In air/liquid, in situ, continuous process Can be manipulated	Large scan area Fast scan speed Cheap	Nanoscale High resolution Fast scan speed	Nanoscale High resolution Fast scan speed	Study dynamic process Fast scan speed 2D and 3D In situ
Disadvantages	Small scan size Slower scan speed Difficult for soft material	Only 2D Need pretreatment Low resolution and magnification	Only 2D Need pretreatment Not native status	Only 2D Need pretreatment Not native status	Complicated operation Need pretreatment

Reprinted with permission from Journal of Food Science 2007, 72, R65-75. Copyright (2007), John Wiley and Sons, Inc. [1].

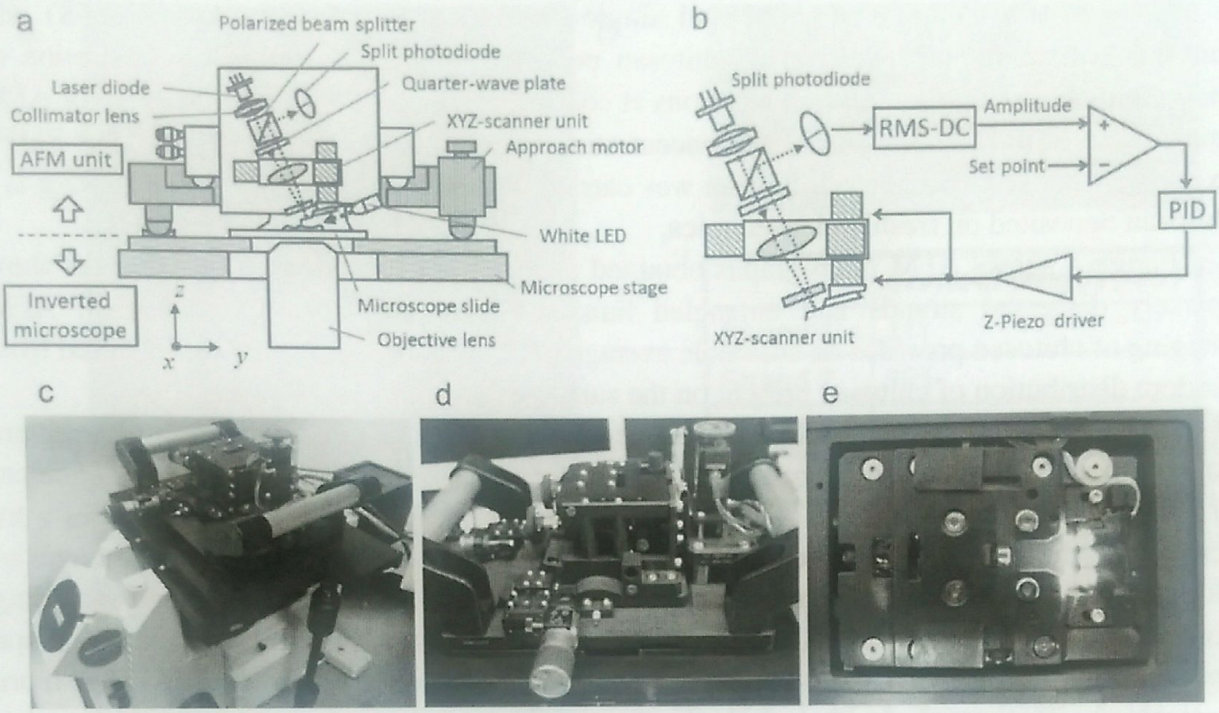

Reprinted with permission from Scientific Reports 2013, 3, 2131. Copyright (2013), Nature publishing group, Inc. [11].

Figure 3. (a) Schematic layout of a high-speed AFM head unit. (b) Block diagram for the feedback loop. (c, d) Overall view of a high-speed AFM head unit mounted on a standard inverted optical microscope (OLYMPUS IX71, Olympus, Tokyo, Japan). (e) Bottom view of the head unit.

2. Structural Characterization of Food and Food Related Macromolecules by AFM

2.1. Single Molecule Atomic Force Microscopy and Force Spectroscopy of Chitosan

Chitosan is a linear cationic polysaccharide with broad biomedical applications due to its excellent properties such as biocompatibility, biodegradability and nontoxicity [13, 14]. It is beneficial for the promotion of chitosan-based biomaterial research to understand chitosan at the single molecule level.

At molecular level, AFM has been proven very successful in the study of probe for desorption of individual chitosan polymer chains. AFM and AFM-based force spectroscopy give lots of information about chitosan with varied chemical composition. Chitosan polymer possessing high level of flexibility and mobility often present the aggregated state expected for a highly positively charged polymer strand. And hence, when chitosan is adsorbed onto a flat mica substrate, elongated single strands or aggregated bundles will be observed in AFM images of chitosan polymer. The elongated single strands are visualized when stable interactions with the substrate are present. Contour length and molecular height, which are two important quantitative information of chitosan, can be obtained from high resolution AFM images [15].

A successful example of AFM and single molecule force spectroscopy (SMFS) was introduced here for investigation of chitosan polymer chains, especially the desorption of individual chitosan [16]. Chitosan solutions at concentration of 0.05 g L^{-1} were used for AFM imaging while the solutions keep the concentration between 0.0007 and 0.05 g L^{-1} for SMFS experiments. AFM imaging of chitosan was carried out under acetate buffer with 0.05 g L^{-1} chitosan deposited on freshly cleaved mica.

Figure 4 shows AFM micrographs obtained under liquid conditions. These images show sparsely dispersed strands and entangled bundles. With drop-casting techniques, AFM imaging of chitosan provides an ensemble average of all possible conformations resulted from random distribution of chitosan present on the surface.

Figure 4a shows AFM images of the same area of a mica surface obtained in intermittent contact mode with chitosan prepared by drop-casting techniques. Little or no rearrangement of the chitosan strands appeared on the mica surface with time when consecutive images were scanned on the same area (Figure 4a). Figure 4b and 4c show high resolution AFM images of elongated chitosan strands on mica surface and present quantitative information including contour length and molecular height values. To determinate molecular width, shape convolution to account for the radius of the AFM tip is commonly required. Thus, it is more straightforward to evaluate the molecular height. Four elongated chitosan strands and a chitosan strand in crosssection is shown in Figure 4b and 4c, respectively. Contour lengths of chitosan strands 1–4 are 111, 121, 94 and 178 nm. respectively while the average value of molecular height of chitosan strand in crosssection is 0.45±0.04 nm.

SMFS has emerged as a powerful tool to investigate the interactions of chitosan with the substrate. The most common force spectroscopy techniques are optical tweezers, magnetic tweezers and atomic force microscopy. Table 2 shows these techniques and examples with regard to their features and limitations [17].

In a typical SMFS experiment, dilute chitosan solutions are drop-casted onto glass slides and then an unmodified AFM tip probes the surface with several hundred approach/retract cycles. Finally, a force curve is obtained to reveal tip-chitosan interaction information [16].

Four typical force curves display desorption events in SMFS experiments with unmodified AFM tip probes. The bridging length between the tip and the surface is 150 nm. When a single and same chitosan molecule arises and desorbes, the force curve retraction pattern and molecular height of the desorption plateau (~100 pN) possess consistent reproducibility. The AFM imaging for long linear strands of chitosan indicates the appearance of the constant force plateaus in force curves.

In a series of SMFS experiments for chitosan with unmodified AFM tip probes, only a few dozen force curves exhibited desorption events while the majority exhibited constant force plateaus out of hundreds of events of SMFS experiments. Therefore, AFM tips covalently modified with chitosan were prepared to eliminate the possibility of measuring chitosan desorption from the tip. This method can simplify the experimental settings on the basis of the amount of chitosan determined in SMFS experiments.

Figure 5 shows typical force curves obtained with a chitosan-modified tip on glass in acetate buffer. Force curves obtained with chitosan modified AFM tips have similar constant force plateau features compared with that obtained with non-modified AFM tips. It is worthwhile to note that plateaus probably appear when the material is desorbing from the AFM tip [18].

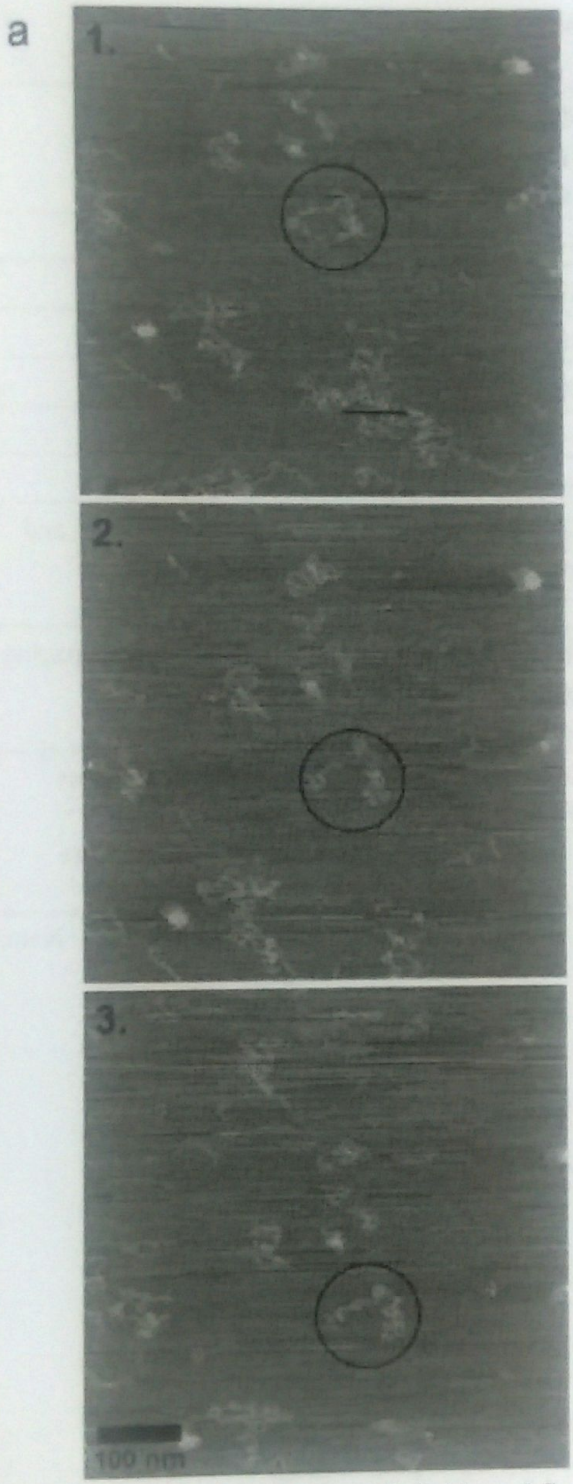

	Contour length (nm)
Strand 1	111
Strand 2	121
Strand 3	94
Strand 4	178

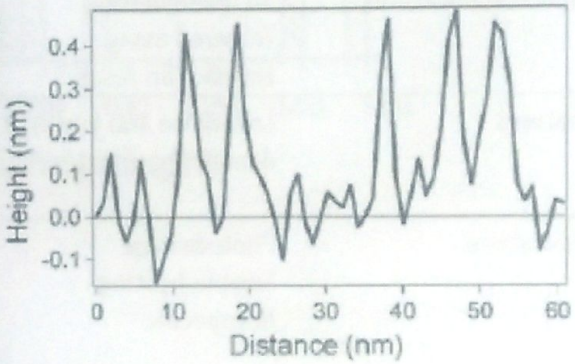

Reprinted with permission from Colloids and Surfaces B: Biointerfaces 2011, 82, 470–476. Copyright (2011), Elsevier, Inc. [16].

Figure 4. (a) 1–3: Consecutive scans of the same area of a mica surface where chitosan (0.05 g L^{-1}) was drop cast. AFM images were obtained in intermittent contact mode in acetate buffer (pH 5.1). Z-scale is 3 nm. (b) Elongated chitosan strands on mica surface with their calculated contour lengths. (c) Height profile of a cross section taken in image (a) 1.

Table 2. Comparison of single-molecule force spectroscopy techniques

	Optical tweezers	Magnetic (electromagnetic) tweezers	AFM
Spatial resolution (nm)	0.1–2	5–10 (2–10)	0.5–1
Temporal resolution (s)	10^{-4}	10^{-1}–10^{-2} (10^{-4})	10^{-3}
Stiffness (pN nm^{-1})	0.005–1	10^{-3}–10^{-6} (10^{-4})	10–10^{5}
Force range (pN)	0.1–100	10^{-3}–10^{2} (0.01–10^{4})	10–10^{4}
Displacement range (nm)	0.1–10^{5}	5 –10^{4} (5–10^{5})	0.5–10^{4}
Probe size (μm)	0.25–5	0.5–5	100–250
Typical applications	3D manipulation Tethered assay Interaction assay	Tethered assay DNA topology (3D manipulation)	High-force pulling and interaction assays
Features	Low-noise and low-drift dumbbell geometry	Force clamp Bead rotation Specific interactions	High-resolution imaging
Limitations	Photodamage Sample heating Nonspecific	No manipulation (Force hysteresis)	Large high-stiffness probe Large minimal force Nonspecific

Reprinted with permission from Nature Methods 2008, 5, 491-505. Copyright (2008), Nature publishing group, Inc. [17].

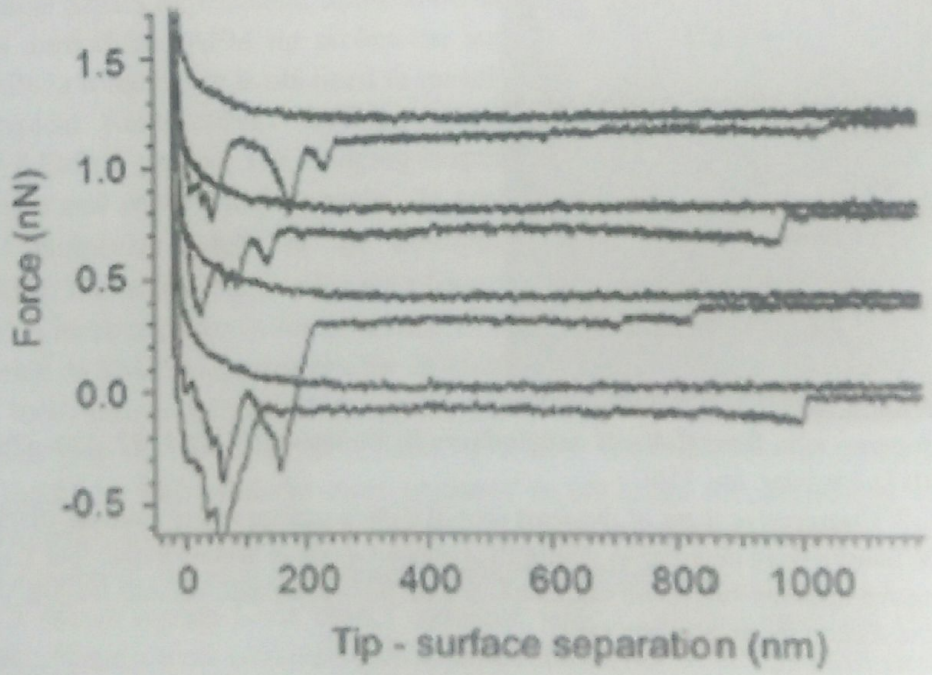

a

Figure 5 (Continued).

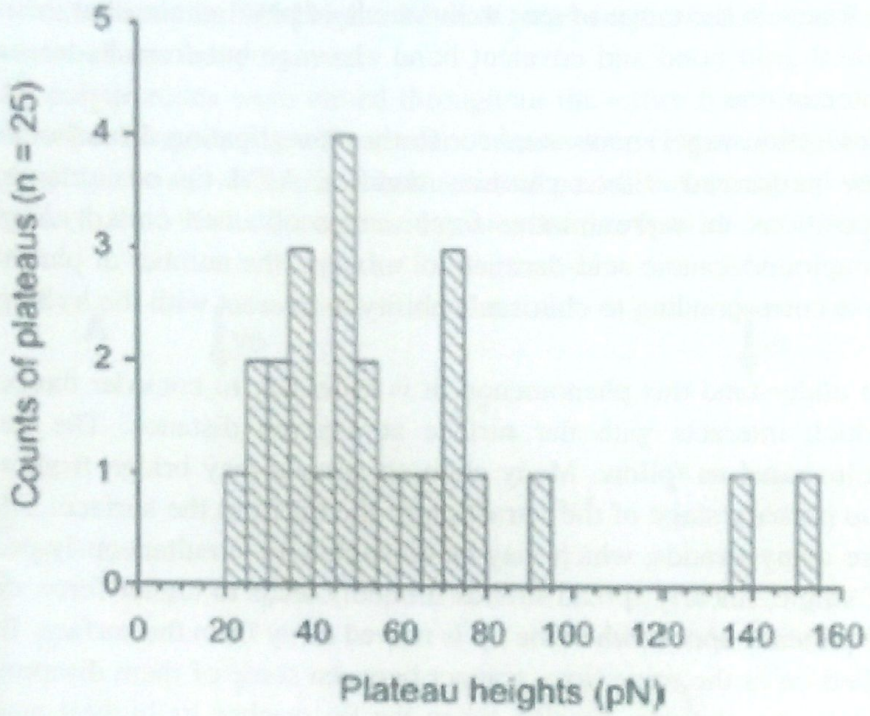

b

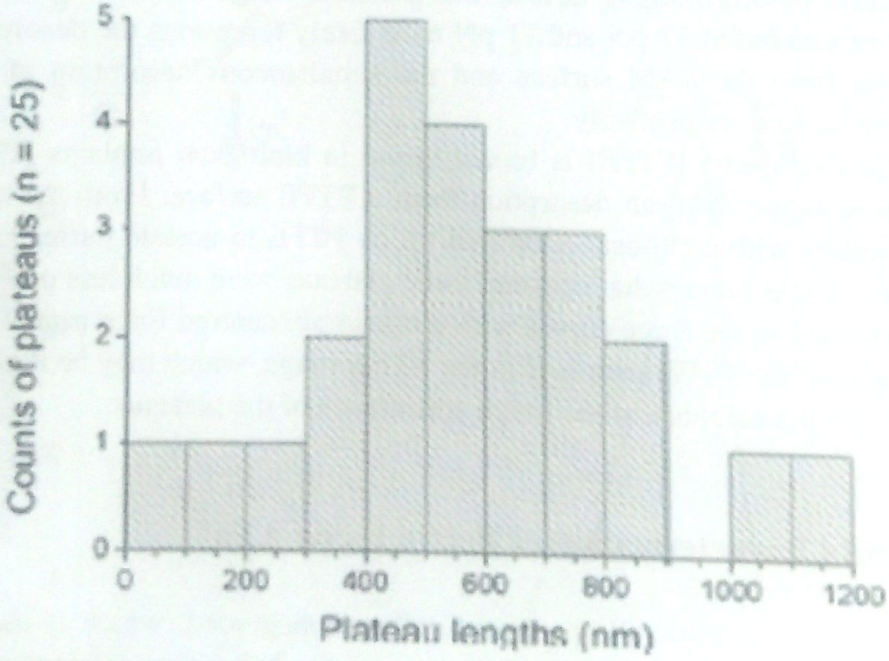

c

Reprinted with permission from Colloids and Surfaces B: Biointerfaces 2011, 82, 470–476. Copyright (2011), Elsevier, Inc. [16].

Figure 5. (a) Typical force curves obtained with a chitosan-modified AFM tip on glass in acetate buffer at pH 5.4 (b) Plateau heights of chitosan strands (immobilized on the tip) desorbed from glass. (c) Lengths of plateaus shown in 4a. The pulling rate was 1 μms^{-1}.

Major force curves exhibit constant force desorption plateaus when a covalently modified tip is used. It is similar to the results obtained without the tip modification. The heights of the plateaus possess good similarity between experiments in which non-modified and modified tips were used.

Generally, forces in the range of tens to hundreds of pNs indicate that interactions are not derived from thiol-gold bond and covalent bond cleavage but from hydrogen bonding and hydrophobic interactions.

Another desorption experiments used for further investigating the adhesive properties of chitosan can be performed with a chitosan-modified AFM tip on surfaces with varying chemical compositions. In representative force curves obtained on a hydrophobic probing surface of mercaptoundecanoic acid-decanethiol mixture, the number of plateaus has varying heights, which is corresponding to chitosan's ability to interact with the hydrophobic probing surface.

In order to understand this phenomenon, it is necessary to consider the possible amount of chitosan which interacts with the surface at a given distance. The multiple plateau desorption is illustrated as follow. Many chitosan strands may bridge from all sides of the cantilever at the primary stage of the retraction of the tip from the surface. The high number of strands cause many strands, which may be entangled, to simultaneously peel. Oppositely, the distance of single, linearly spread strands limitedly leads to higher-force shorter plateaus. Changes of the plateaus appear when the tip is moved away from the surface. Because several strands are pulled on at the same time, contact between some of them disappear, which then causes stepping in the plateaus. Finally, when the tip reaches its highest position from the surface, long constant plateaus appear in the force curves because only the longest strand can remain interaction before bridging is lost. The plateaus' heights can be quantified into two peaks. The force centred at 37 pN and 71 pN most likely represents the desorption of single chitosan strands from the SAM surface and the simultaneous desorption of two chitosan strands from the surface, respectively.

Polytetrafluoroethylene (PTFE) is broadly used in biological implants [19]. Thus, it is important to investigate chitosan desorption from a PTFE surface. From the comparison of force curves probed with a chitosan-modified tip on PTFE in acetate buffer to the previous surfaces studied, it was known that constant force plateaus were much less uniform; although they can be observed in the force curves with a maximum centred force around 100 pN. The surface roughness of the PTFE sample is in the 10 nm range, which may be the reason for the broad range of plateau heights and the rough appearance of the plateaus.

2.2. Structural Characterization of Pectin Using AFM

With the ripening of fruit, the pectin of cell wall degraded, which is the main reason leading to fruit softening [20, 21]. The changes of structural characterization of cell wall pectin could be demonstrated by AFM. AFM can image pectin's molecules and polymers directly, thereby it has been used to study plant materials comprehensively, including sodium carbonate-soluble pectin, chelate-soluble pectin (CSP), water-soluble pectin and cell walls. The images of AFM have revealed information about morphological arrangement such as branching, height, width and cell wall structure. With AFM, we can analyze the changes of pectin characteristics qualitatively and quantitatively.

It is often necessary to investigate some molecular features such as sugar profiles before performing the AFM experiments. Figure 6 shows the uronide and neutral sugar profiles

obtained from pectin fractions. The bright and dark areas correspond to peaks and troughs in the images of pectin chains and polymers.

At one side, polyuronides were eluted throughout the entire fractionation in the CDTA fraction, with three peaks appearing with similar concentration (Figure 6A). On the other side, the neutral sugar polymer showed three small residual peaks, but the signal was low (Figure 6B). This conforms to the ~90% of uronic acid content of this fraction.

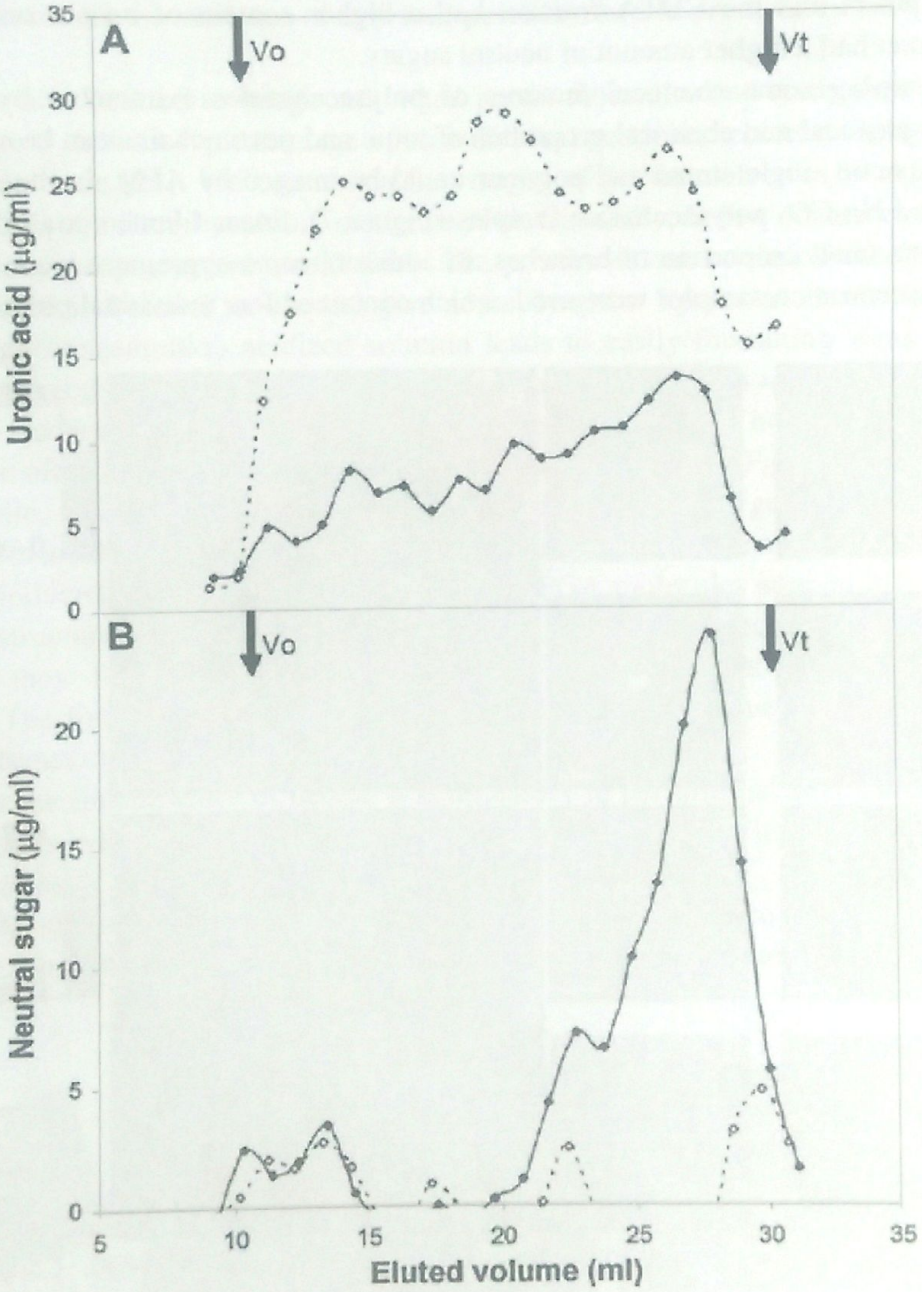

Reprinted with permission from Carbohydrate Polymers 2012, 88, 882–890. Copyright (2012), Elsevier, Inc. [23].

Figure 6. Comparative SEC molecular profiles of polysaccharides extractable by CDTA(dashed lines) and Na_2CO_3 (filled lines) solutions from cell walls of ripe strawberry fruits obtained by SEC on Sepharose CL-2B columns. Fractions were assayed for uronic acid (A) and neutral sugar (B) content. Void volume (V_0) and total volume (V_T) are indicated on the figures.

As might be expected, the concentration values for the polyuronide profile of the Na_2CO_3 fraction were lower than the CDTA fraction (Figure 6A). A small first peak eluted closed to 15 ml but the main peak closed to 27.5 ml. This indicated that the fraction had relatively a lot of low molecular mass polymers. The most important thing was that a sharp peak at the same elution volume was resolved in the neutral sugar profile (Figure 6B). Therefore it can be postulated that this fraction had a higher amount of neutral sugar compared with the CDTA fraction. As a result, the SEC analysis revealed the main differences between CDTA and Na_2CO_3 polymers and the CDTA fraction had a higher content of uronic acids while the Na_2CO_3 extract had a higher amount of neutral sugars.

After learning some chemical features of polysaccharides extractable by CDTA and Na_2CO_3, the physical and chemical properties of ionic and pectin chains can be carried out by AFM. Both pectin single strand and polymer could be imaged by AFM. In the AFM images of CDTA and Na_2CO_3 polysaccharide samples (Figure 7), linear filamentous structures were observed with small proportion of branches. In addition, some aggregates were also imaged, even low concentration samples were used, which contained few individual polymers.

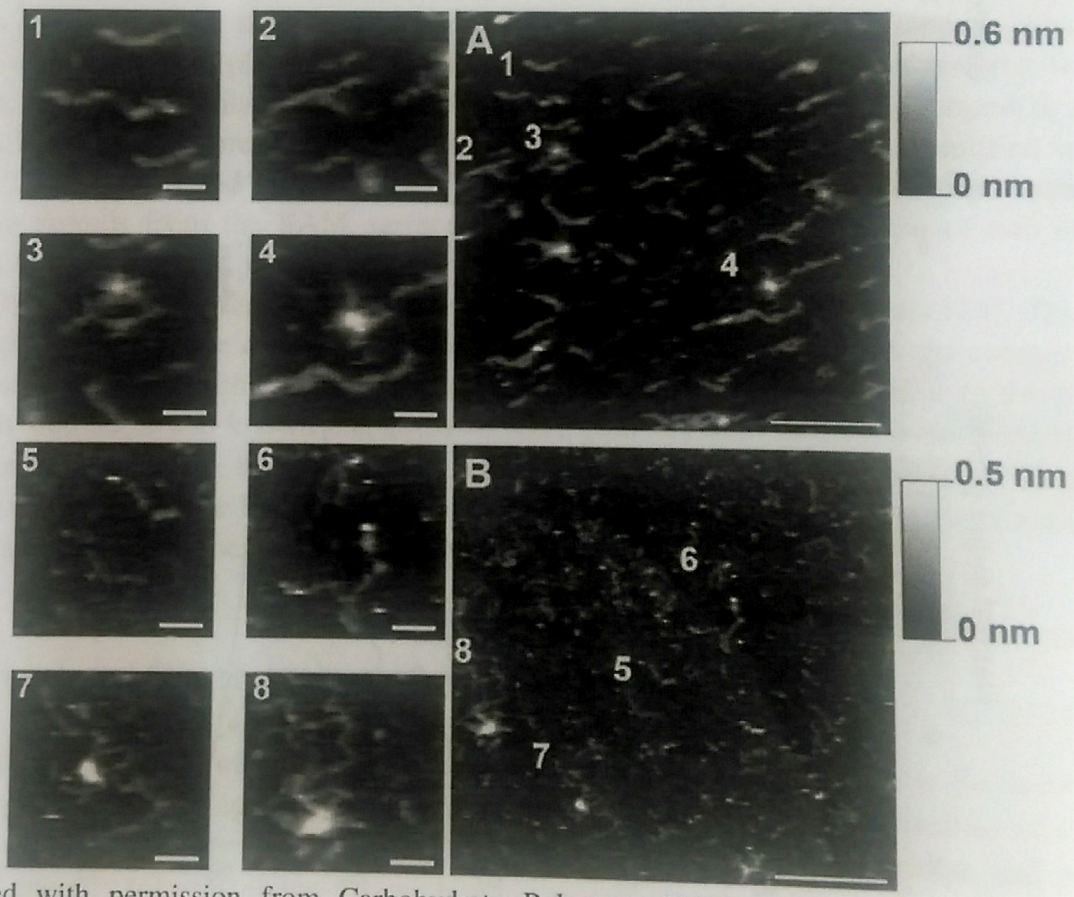

Reprinted with permission from Carbohydrate Polymers 2012, 88, 882–890. Copyright (2012), Elsevier, Inc. [23].

Figure 7. Representative topographical AFM images of CDTA (A) and Na_2CO_3 (B) pectin extracts after drop deposition onto mica. Inserts (1–8) show zoomed areas from the A and B images to show examples of single linear chains (1 and 5), branched chains (2 and 6) and aggregates or multi-polymer complexes (3, 4, 7 and 8), respectively. AFM images are accompanied by height scale bars showing the dz value (highest height during the scan). The scale bars for A–B are 250 nm, whilst the scale bars for the inserts 1–8 are 50 nm.

This observation indicated that they are not simply superpositions or entanglements of polymers caused by the reduction of solvent volume, but are multi-polymer complexes hold together by intermolecular interactions. The presence of these polymers and aggregates reflects the heterogeneity and complexity of the pectin polysaccharides present in cell wall fractions.

Therefore, the changes of structures of cell wall pectin fractions extracted from strawberry with the extension of time can be clearly analyzed by AFM to observe enzyme actions, which makes the structure of cell wall pectin broken to promote the fruit mature and soft.

AFM can also be used to image individual pectin molecules and study their aggregation usually. Figure 8 shows a typical image of an individual pectin molecule: an image of a sugar beet pectin molecule [24]. We can obtain the images of pectin molecules in aqueous media and $MgCl_2$. Gels can form by adding moderate acid. Generally, in low concentration acidized solution, fibrous gel precursors would form. The precursors can be deposited onto mica and imaged by AFM in butanol media and give some irregular figures as shown in Figure 8b. However, high concentration acidized solution leads to easily formatting weak gels which were imaged directly. In addition, these gels could be easily broken to fragments of gel and then this gel fraction would be isolated and deposited onto mica. Thus when imaging these structures, we often find that it might be branched fibrous networks (Figure 8c).

Meanwhile, similar structures are observed in calcium-induced gels. The branched fibre structures from a calcium-induced alkali-treated sugar beet pectin gel are similar to those seen for the acid-induced structures. Thus the studies on PGA molecules support a fibrous model for the gel structure. It is a common opinion that the PGA molecules are fully charged. Expectedly, they form into fibres to accomplish the neutralisation of the charge on association. The formation of fibres doesn't depend on a continuous distribution of charge along the polymer chain.

To study the functionality of pectin, it is necessary to perform gelation studies aiming at the RGI regions which might act as discontinuities and could influence branching of the fibrous structures.

Figure 9a shows obvious advance and retract curves by force spectroscopy. Lectin-carbohydrate binding was obtained in the study involving interaction between mRGI and Gal3.

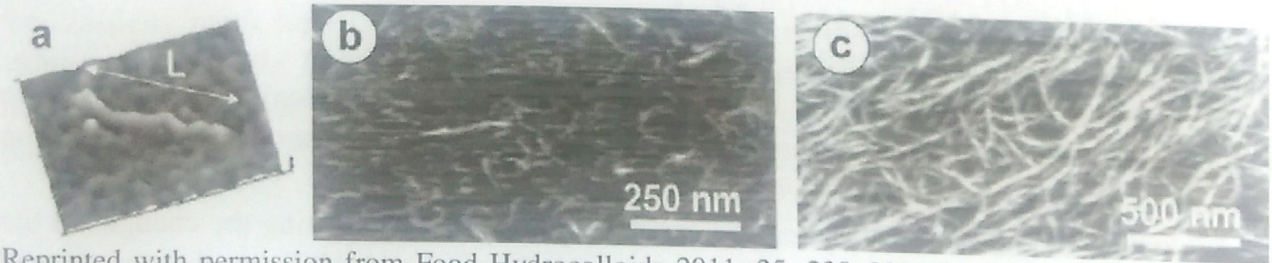

Reprinted with permission from Food Hydrocolloids 2011, 25, 230–237. Copyright (2011), Elsevier, Inc. [24].

Figure 8. AFM images of sugar beet pectin, acid-induced gel precursors and gels formed following de-esterification of the pectin. (a) Topography image of an individual pectin molecule imaged in the presence of $MgCl_2$. The mean length for the population of molecules was found to be $<L> = 70$ nm. (b) Topography images of pectin molecules and fibrous gel precursors imaged under butanol. (c) Topography image of a fragment of an acid-induced gel imaged under butanol.

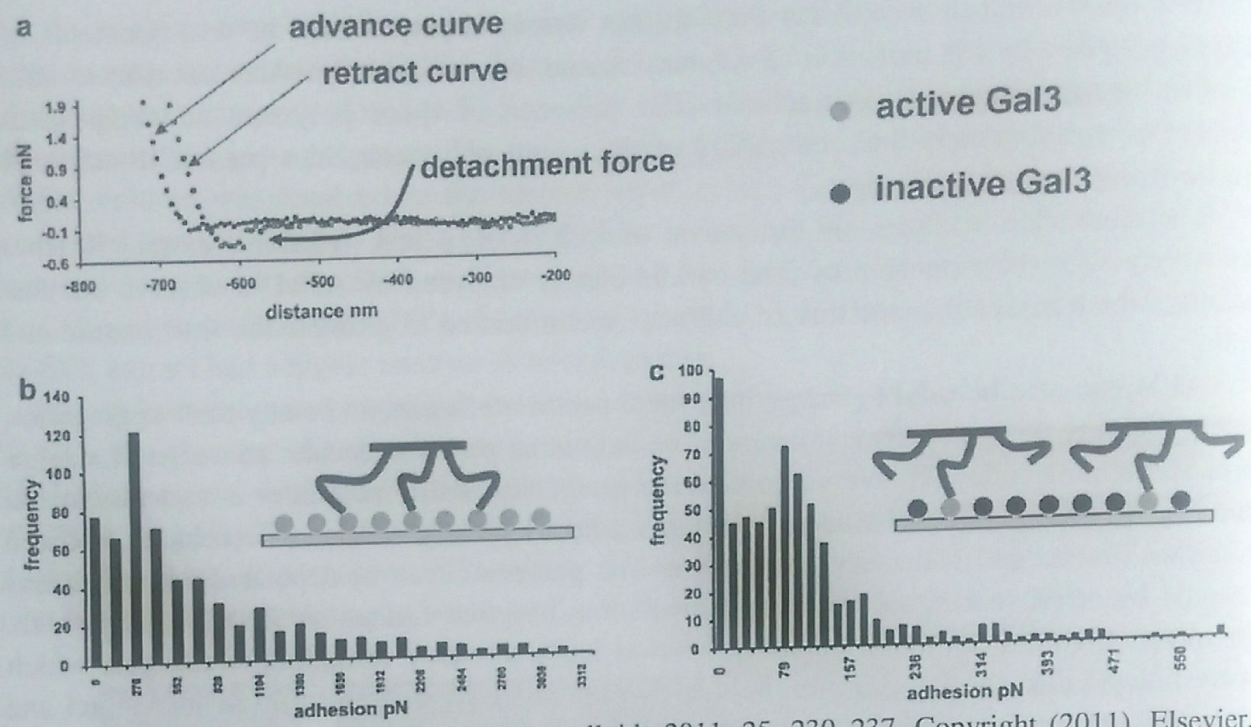

Reprinted with permission from Food Hydrocolloids 2011, 25, 230–237. Copyright (2011), Elsevier, Inc. [24].

Figure 9. Force spectroscopy data on Gal3-mRGI interactions. (a) force-distance curves showing a binding event. (b) Histogram of the frequency of measured binding events - insert shows suggested binding of mRGI to immobilised active Gal3. (c) Histogram of the frequency of measured binding events after partial inactivation of Gal3 with added lactose-insert shows suggested binding of mRGI to immobilised active Gal3.

The detachment force corresponds to the interaction between Gal3 and mRGI (Figure 9a). Alternatively, Figure 9b and Figure 9c show a clear histogram about the binding events and the value of the detachment force, which was calculated to be about 276 pN. So the specific-formation of pectin structure and detail functionality of pectin may be effectively investigated by using AFM and force spectroscopy.

2.3. Imaging Living Cells Surface and Quantifying Its Properties at High Resolution Using AFM in QI™ Mode

Atomic Force Microscopy has been used as a useful tool in biology to investigate the living cells for their morphology, surface roughness and nanomechanical properties based on classical imaging modes known as contact mode and tapping mode.

In contact mode, AFM measured the sample topography by detecting the changes in the deflection of the tip as it scans over the sample and a function of position on the surface was established in terms of height [25].

However, the AFM tip would deform the surface of deformable soft samples, which may cause that the topographic images poorly correlated with the variations in height. Taping mode can be used to image soft sample by employing a stiff cantilever which is oscillating near its resonance frequency during the scan without contact with the sample, whereas the contact between the sample and the tip is unavoidable for the oscillation amplitude that can be

influenced by the forces of a biological system where the electrolyte concentration is high [26]. In addition, interactions with low-range surface forces affect the vibrating tip during its trajectory. High speed AFM and multi-frequency force spectroscopy were developed to image sample faster by increasing the scan rate. However, these two modes also need oscillating tip thus high speed AFM and multi-frequency force spectroscopy is hardly used to study the biophysical properties.

Force-volume (FV) (also known as force mapping) mode have been proposed to measure mechanical properties and image cells in liquid conditions without changing their cell surface or removing from the substrate for the tip. However, the FV mode exist difficulties while working on short term effect with living cells under physiological conditions for the time needed to acquire each force curve. In the other hand, the FV mode does not produce accurately precise images, which may lead to misunderstand of the result for its low resolution [27].

A new advanced mode is quantitative imaging (QI™) based on force curve acquisition [28]. This mode allows applying in samples such as soft or loosely bound ones and its force curves can be collected at the same speed with resolution as normal imaging. In this mode, force curve is recorded for each pixel thus it allows acquiring both mechanical properties and topography data at the same time and same sample.

Figure 10 shows a successful example using the quantitative imaging (QI™) to image and measure soft sample and loosely immobilized ones in liquid. Figure 104a-d shows the images of loosely immobilized micro-organisms and organelle using different methods. Figure 10a presents an image of bacteria which barely withstand the lateral force exerted by the scanning tip of contact mode. Figure 10b shows the image of *E. coli* cells which can precisely give the cell dimensions. The dimensions can be calculated from the point of contact on each force curve. From Figure 10c, we can see that the E. coli samples can be scanned at the beginning but soon the scanning tip removes the cell from its hole. Figure 10d shows the high resolution "zero-force" height image of the entire cells obtained by the QI™. Figure 10e shows the deformed nucleus of bacteria and yeast by the contact mode. While Figure 10f indicated that imaging of nucleus can be obtained by QI™ mode when nucleus is on PDMS without any electrostatic immobilization.

QI™ mode is not only useful for imaging difficult samples but also useful for nanomechanical measurements on soft sample and loosely immobilized ones in liquid. Figure 11a and d describe the direct correlation between height images; Figure 11b, c, e and f present the elasticity maps for HCT116 and C. albicans cells with showing the distribution of YM values on the sample. In each case, the same data were recorded using QI™ mode (Figure 11c and e) and FV mode (Figure 11d and f). QI™ mode gives higher resolution images and allows a detail view of the sample due to the number of record force curves.

2.4. Characterization of and Manufactured Nanoparticles by Atomic Force Microscopy

Polymeric micro- and nano-fibers, nanotubes and nanorods are useful for a wide number of applications [29-32]. Polymers filled with nanomaterials (e.g., carbon nanotubes) have

been investigated in order to reveal structures with enhanced mechanical and/or electrical properties to improve the performances of the devices.

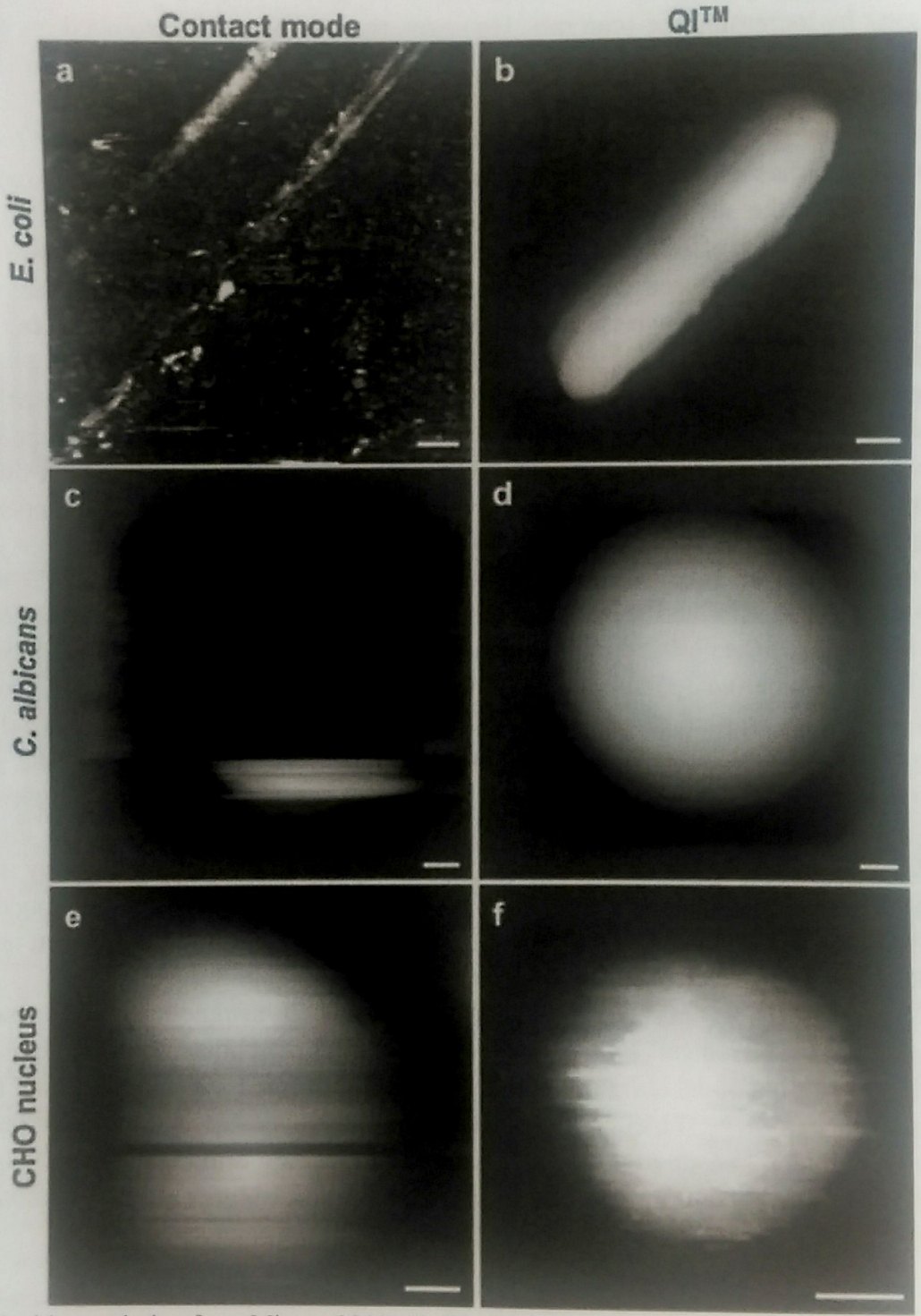

Reprinted with permission from Micron 2013, 48, 26–33. Copyright (2013), Elsevier, Inc. [28].
Figure 10. Imaging of loosely immobilized samples. Contact height image (resolution: 512 lines) of (a) an E. coli cell (z-range = 1.2 µm, (c) a C. albicans cell (z-range = 2 µm) and (e) of a CHO nucleus (z-range = 1.8 µm). QI™ height image (256 px^2) of (b) a E. coli cell (z-range = 20 nm), (d) a C. albicans cell (z-range = 2 µm) and (f) a CHO nucleus (z-range = 2 µm). The QI™ height images correspond to the contact height images. Scale bar a–d: 0.5 µm; e and f: 2µm.

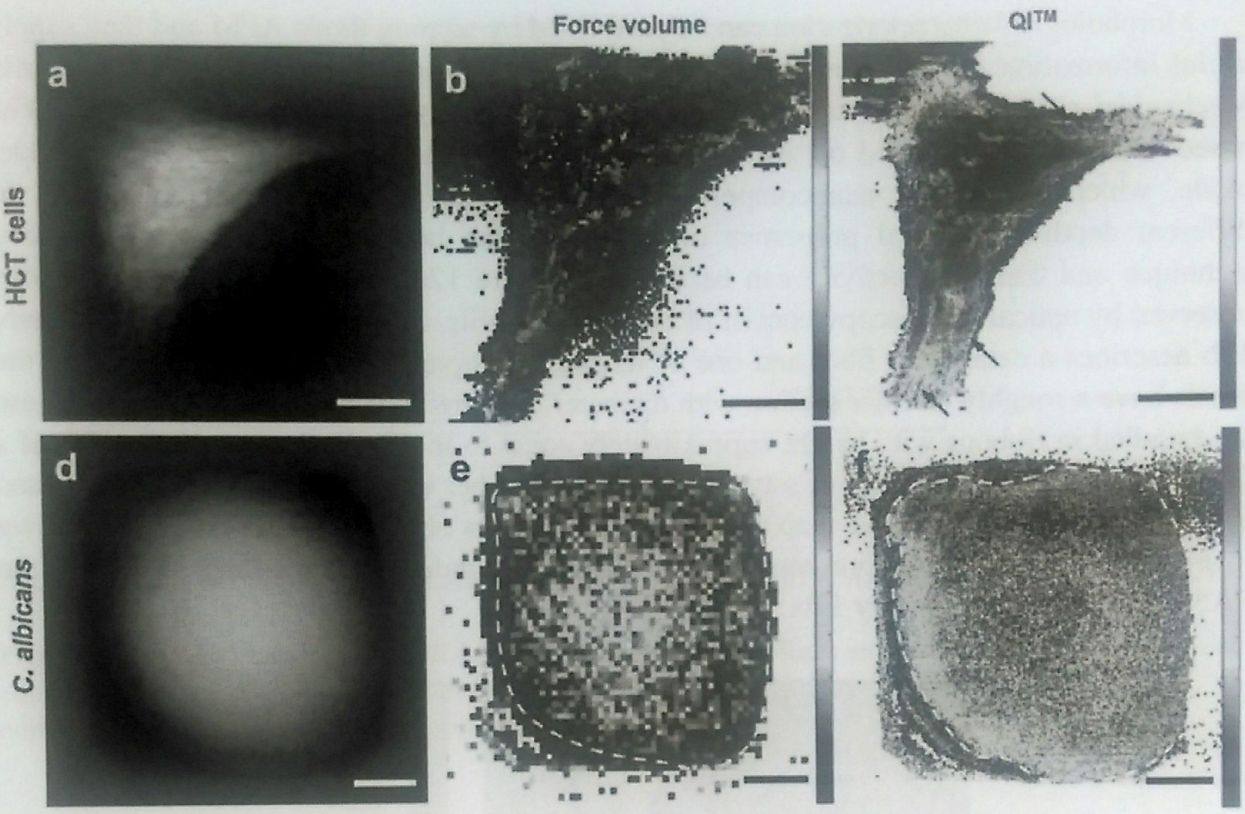

Reprinted with permission from Micron 2013, 48, 26–33. Copyright (2013), Elsevier, Inc. [28].

Figure 11. Mechanical properties. QI™ height image (256 px^2) of (a) an HCT116 cell (z-range = 7 µm). (b) Force volume elasticity map (128 px^2) of the same HTC116 cell (YMscale = 0-10 kPa). (c) QI™ elasticity map (256 px^2) of the same HTC116 cell (YM-colorscale = 0-10 kPa). Arrows show the stress fibers revealed by QI™ measurement. (d) QI™ height image (256 px^2) of a C. albicans cell (z-range = 2 µm). (e) Force volume elasticity map (64 px^2) of the same C. albicans cell (YM-colorscale = 0-500 kPa). White dashed line circles the region of interest. (f) QI™ elasticity map (256 px^2) of the same C. albicans cell (YM-colorscale = 500 kPa). White dashed line circles the region of interest. a-c:10 µm, scale bar d-f: 1 µm.

Much attention has been drawn to Polyaniline (PANI) for its conductively effects [33]. However, it is difficult to characterize the properties of nanocomposite PANI fibers and other nanocomposite polymeric structures. In particular, the study of samples properties at nanoscale requires techniques being able to probe the surface with nanometrical lateral resolution.

Atomic force microscopy (AFM) has been proposed as a tool to develop techniques for mapping various physical properties simultaneously to the morphological reconstruction with nanometrical lateral resolution for it can probe the sample by using a tip with radius of few nanometers placed in close vicinity of the sample surface. Moreover, AFM tip can exerts a force on the sample surface as a consequence of the deflection of the cantilever and allows one to investigate the mechanical properties of the volume of the sample quickly under the tip. Using tips and cantilevers coated with conductive substrates and conductive ultra-thin films, electrical properties of the sample can be characterized by the record of corresponding electric which is generated by the voltage between the tip and the sample.

The morphological, mechanical and electrical characterization of nanocomposite fibers from chemical polymerization of PANI/DND nanocomposited was successful performed by advanced atomic force microscopy (AFM) [34].

Morphological characterization can be performed by tapping mode AFM and then supply useful information for the structure of fibers and ribbons forming the PANI/DND network. Mechanical characterization can be carried out synergically by using two different AFM based techniques, one based on AFM tapping mode and the other based on AFM contact mode, which probed the nanocomposited nature of PANI/DND fiber sample down to different depths. Electrical properties of the fibers can be assessed by an AFM based technique and their conductivity can be verified. Figure 12a shows the fibers and ribbons observed by optical microscopy consist of bundles of fibrils, either parallel or twisted. Figure 12b describes a detail of a fiber and one of its cross sections. This figure indicated that the fibrils have a roughly circular section with diameter of a few hundreds of nanometers. These are bundled in ribbons with height approximately equal to the fibril diameter and width of a few microns. The morphology of a typical PANI/DND fiber was presented in Figure 13a and the corresponding quantitative map of indentation modulus obtained by TH-AFM was shown in Figure 13b. Figure 13c presents the statistics of the indentation modulus values of the PANI/DND fiber retrieved by 13b.

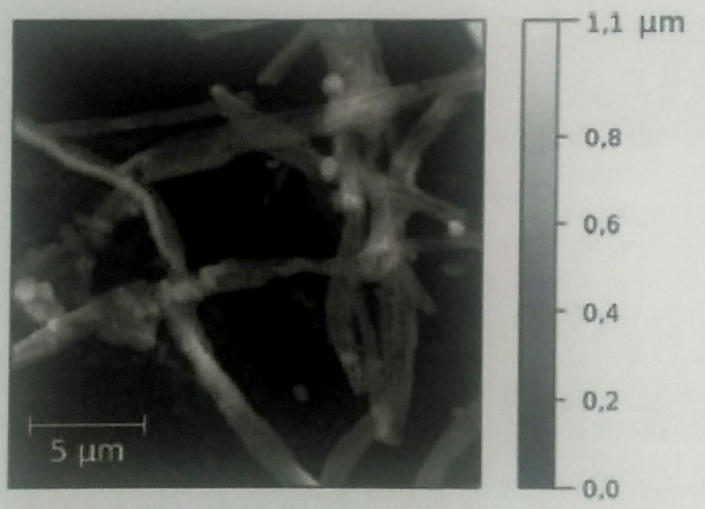

a

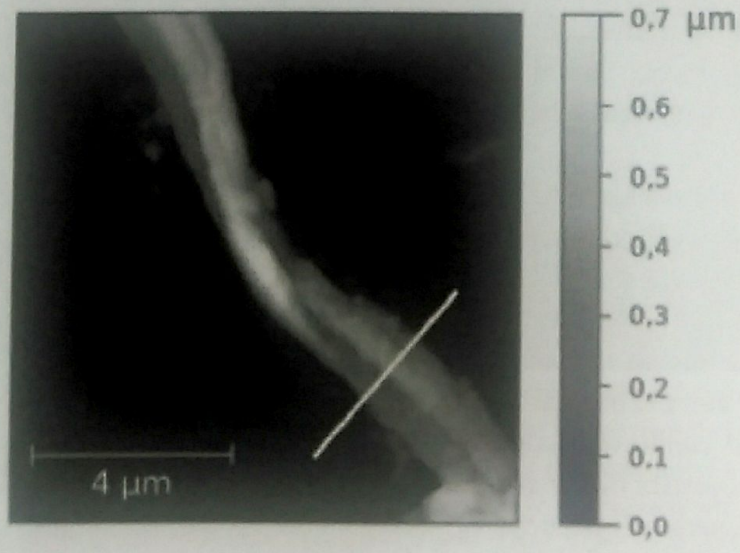

b

Figure 12 (Continued).

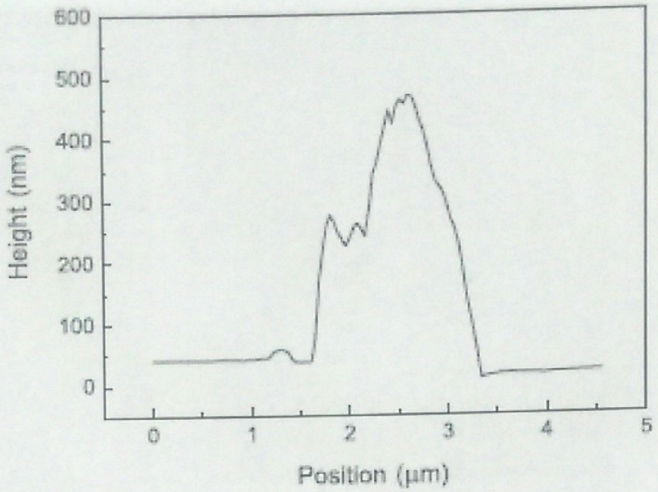

c

Reprinted with permission from European Polymer Journal 2013, 49, 991–998. Copyright (2013), Elsevier, Inc. [34].

Figure 12. (a) AFM image of PANI/DND sample, showing that fibers and ribbons forming the network consist of bundles of fibrils. (b) Detail of a PANI/DND fiber and (c) cross section profile in correspondence of the white segment in (b).

2.5. Spectroscopy and Atomic Force Microscopy of Biomass

One way to investigate feature of biomass is to obtain atomic resolution images. AFM techniques are tremendous importance to perform this analysis. Systematic understanding of the plant cell wall architecture might be acquired by AFM-based techniques. The diversity of biomass can be studied by the several modalities of AFM. There is an example to perform topography and subsurface imaging by using AFM and mode synthesizing atomic force microscopy (MSAFM) [35].

Measurements were carried out for various preparations of both Populus and switchgrass samples including coarsely ground chips of wood and switchgrass (Figure 14), and cross sections of petiole or leave stalk and *Populus* stem tissue (Figure 15)

The cell wall boundary (CW), middle lamella (ML), and globular features of the lignocellulosic structure are clearly visible in the surface morphology of shavings images of Populus cells obtained by tapping mode AFM. However, it is not possible to differentiate between primary and secondary cell walls.

Figure 14 shows an example of switchgrass images obtained by tapping mode AFM. The shavings images of switchgrass samples can not accurately resolve the cell wall structure because that the coarsely ground chips of Populus wood and switchgrass shavings were too rough and difficult to image a large area. However, these images are obtained from native samples. So, we can keep a perspective on the actual lignocellulosic structure biomass based on this kind of images.

MSAFM is a particular mode of AFM and able to use mechanical excitation of the probe and the sample to access the physical information of materials [36]. Figure 15 depicts regular contact mode AFM and MSAFM images of a cross section of Populus wood. For those plant cell walls that the topography is difficult to resolve, the MSAFM images can give more details and reveal new information about the structure.

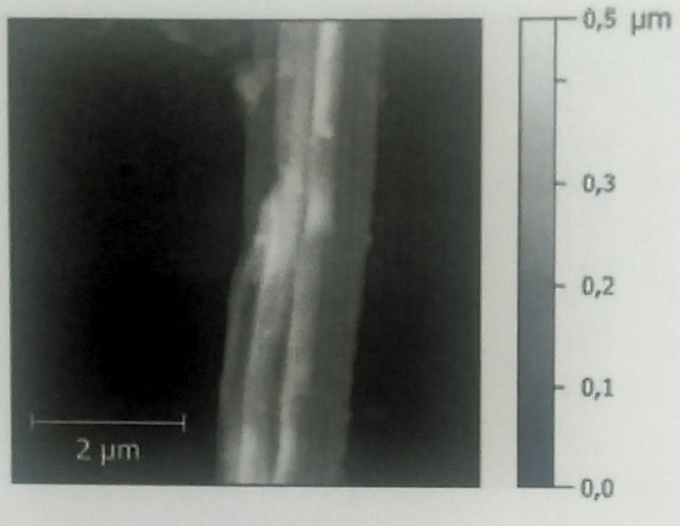

a

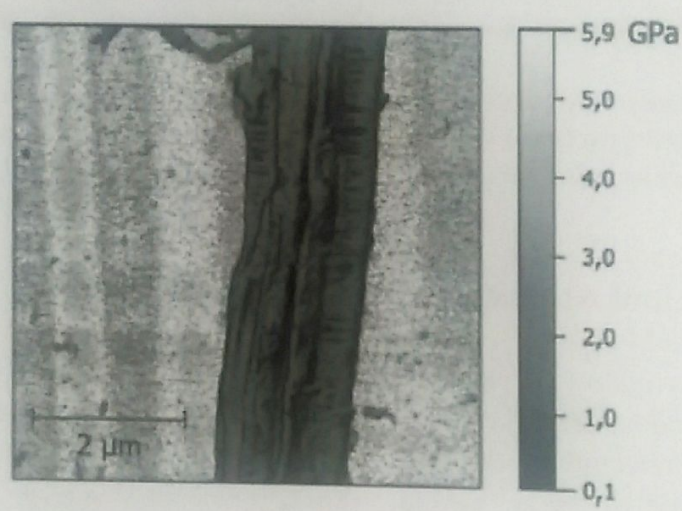

b

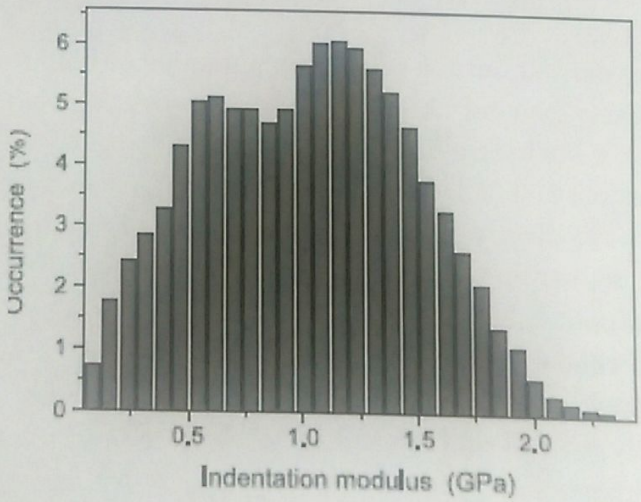

c

Reprinted with permission from European Polymer Journal 2013, 49, 991–998. Copyright (2013). Elsevier, Inc. [34].

Figure 13. Morphology (a) and corresponding quantitative indentation modulus map (b) of a typical PANI/DND fiber, obtained by TH-AFM. (c)Statistics of the indentation modulus values reported in (b) in correspondence of the PANI/DND fiber.

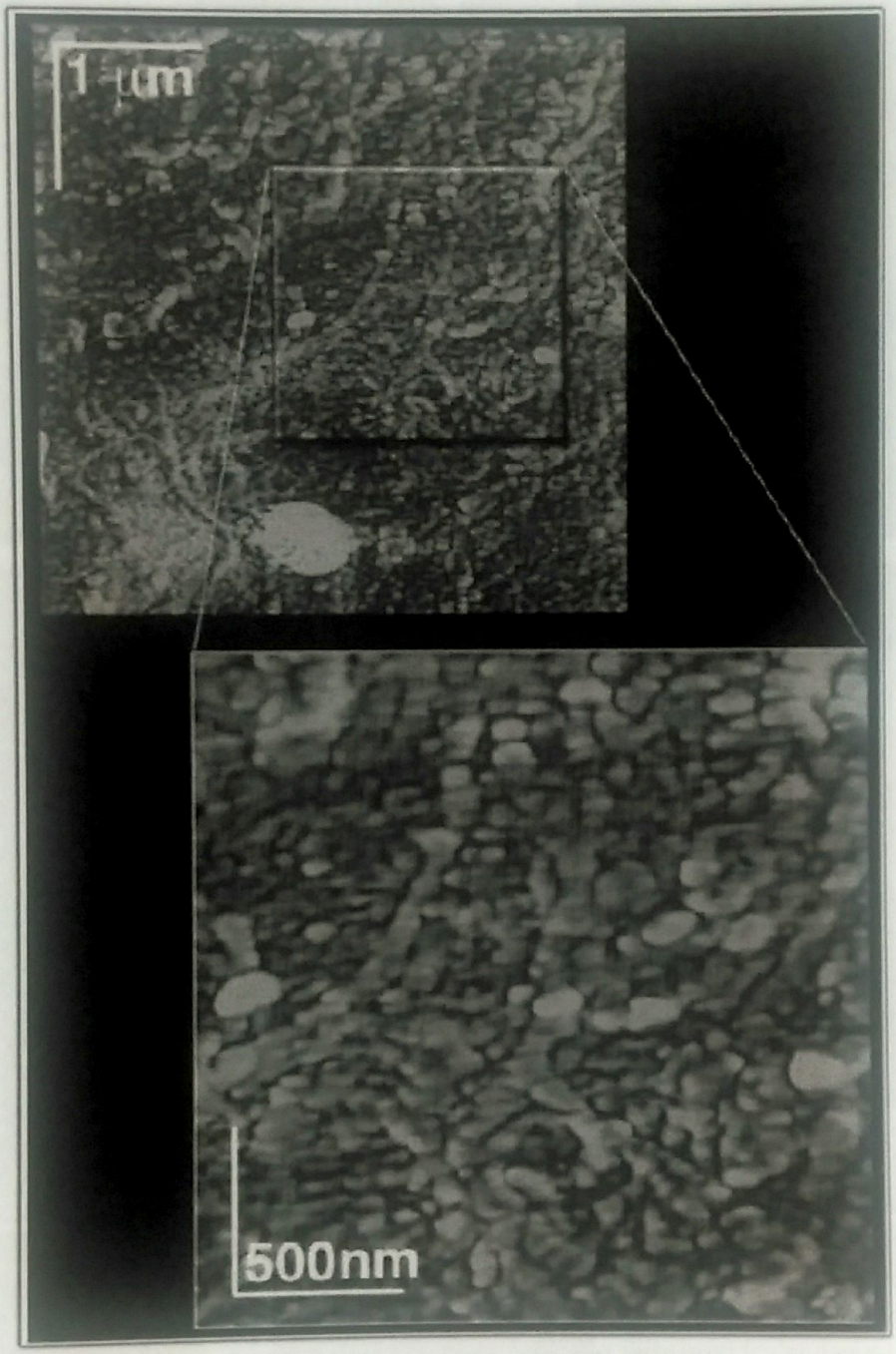

[35].

Figure 14. AFM images of switchgras shavings. Phase data (obtained by Tapping mode) is presented. The macromolecular globules structures attributable to lignin are visible. With the coarsely ground shavings of Populus wood and switchgrass, the samples were too rough to accurately picture the cell wall structure. The unevenness of the samples made it challenging to image a large area.

Figure 15(b) and (d) show materials of various mechanical properties within the cell wall. In fact, Figure 15(d) obviously reveals the difference in the structure of the different layers. The secondary cell wall and fibrous materials can be clearly observed on the right hand side of the yellow dashed line, while the regions of different density are visible on the left hand side of the line.

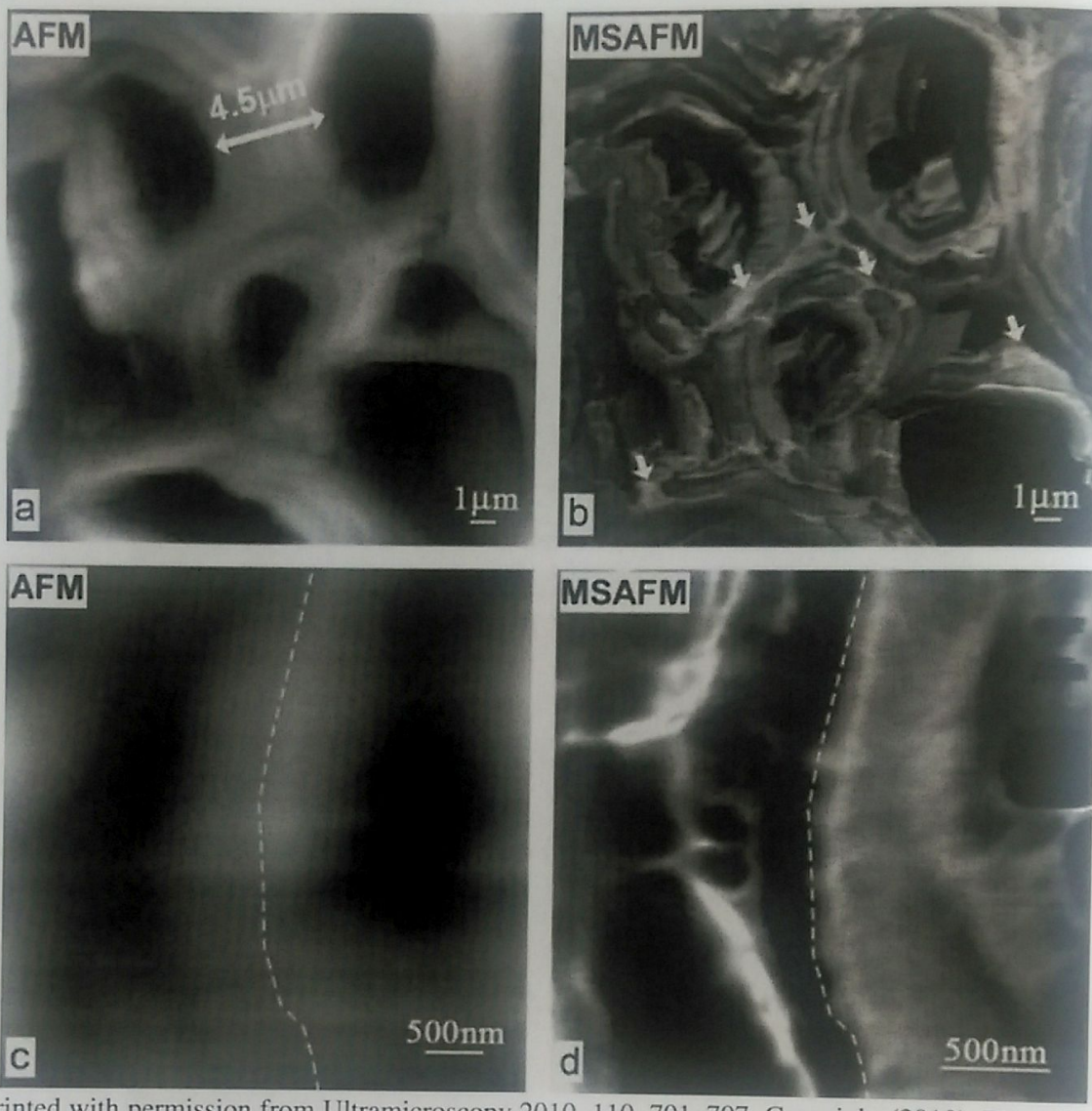

Reprinted with permission from Ultramicroscopy 2010, 110, 701–707. Copyright (2010), Elsevier, Inc. [35].

Figure 15. AFM (left) and MSAFM (right) images of a cross section of Populus wood. MSAFM images exhibit different information from regular topography. The two complementary techniques should be used in order to determine the structural and mechanical properties of the lignocellulosic samples. The arrows indicate the brighter areas of the cell walls, corresponding to the Middle Lamella (ML), which exhibit different mechanical properties revealed by MSAFM.

2.6. Study of Milk/K-Carrageenan Mixtures by Atomic Force Microscopy

Milk/k-carrageenan mixtures can be imaged with AFM at jumping mode and a good image with high resolution can be obtained as long as extreme care was taken when scanning repeatly samples to avoid "shaving" [37].

Figure 16 shows typical AFM images and image analysis of milk plus 0.0001% w/v k-carrageenan samples. In this study, several kinds of samples are adsorbed on highly ordered pyrolytic graphite (HOPG) and mica substrates. With comparing the effects between these two substrates, there are some differences being founded on HOPG and mica surfaces about the adsorption of casein micelles.

Figure 16a and b show an HOPG image which contains a little area scanned six times previously and some small structures observed in the centre. Measuring the height profile in a section was performed through repeated scanning the single surfaces. It can be observed that small structures were "shaved" (Figure 16.c). In the same way, mica images prove the results of "shaving" as shown in Figure 16.d, e and f. Casein micelles could be adsorbed by HOPG fully but adsorbed by mica poorly. The images of casein micelles adsorbed on HOPG can observe pseudo-spherical structures due to the formation of aggregates.

2.7. Morphological Analysis of High-Impact Polypropylene Using AFM

Although micro-computed tomography can effectively characterize the macropores in the entire particles and spatial distribution of ethylene-propylene rubber (EPR) macrozones, it is also important to map the smallest EPR zones and micropores to completely describe the high-impact polypropylene (hiPP) morphology. AFM, an excellent technique visualizing micro- and nano-sized pores and EPR domains, can successfully realize this purpose [38]. Figure 17 shows the AFM phase image of hiPP sample and the AFM topological image of the same area. AFM phase image displays both EPR and pores by dark color (Figure 17a) while AFM topological image displays the pores by the darker color than the EPR phase (Figure 17b).

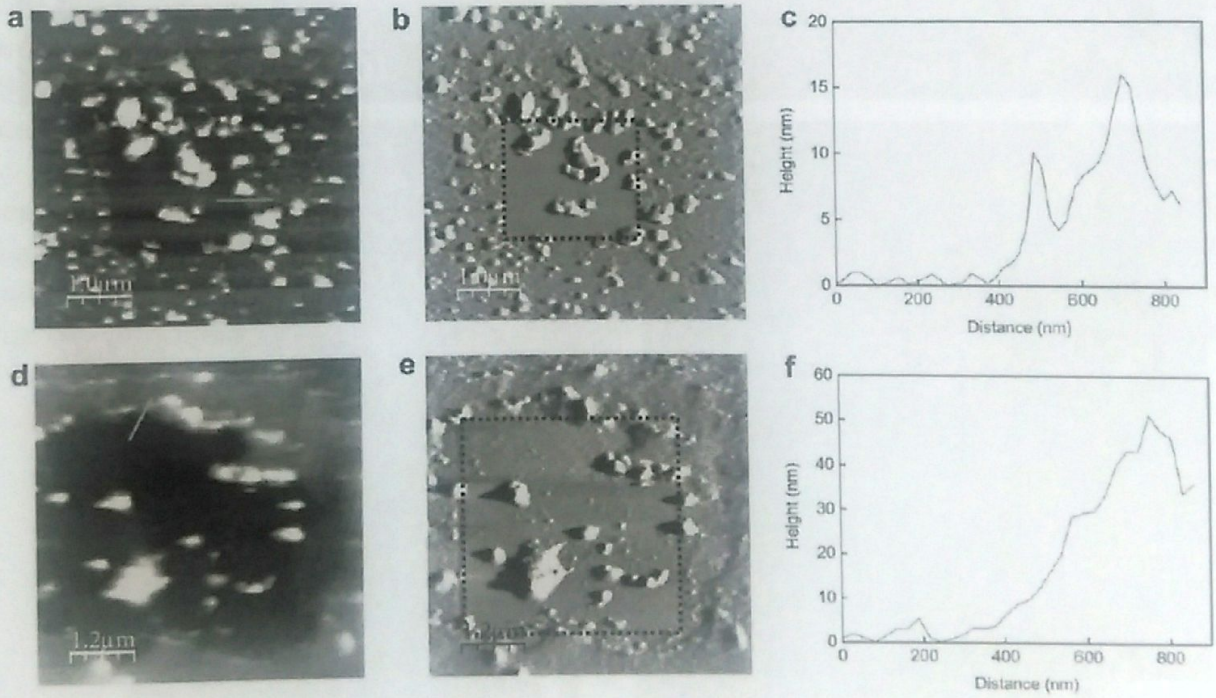

Reprinted with permission from Food Hydrocolloids 2010, 24, 776–782. Copyright (2010), Elsevier, Inc. [37].

Figure 16. Representative AFM images and image analysis of milk plus 0.001% w/v of κ-carrageenan samples: (a) topographical image of a sample adsorbed on HOPG (5 μm × 5 μm); (b) equivalent error signal mode image corresponding to (a); (c) height profile analysis of the cross-section highlighted in (a); (d) topographical image of a sample adsorbed on mica (6 μm × 6 μm); (e) equivalent error signal mode image corresponding to (d); (f) height profile analysis of the cross-section highlighted in (d); (f)height profile analysis of the cross-section highlighted in (d).

AFM phase imaging can not distinguish the EPR phase from the pores and the eventual gaps between particle surface and resin while AFM topological image the pores are situated deeper than EPR phase in AFM topological image. AFM images provide a very clear contrast between soft amorphous EPR phase (dark areas) and hard semicrystalline iPP (bright area) when phase shift of the resonance amplitude signal is displayed in the tapping mode (Figure 17). With setting the threshold, the deepest holes were covered in the topological image and the mask was created to directly recognize the pores in AFM phase image (colored by green in Figure 17c). When the mask is overlaid above the phase image, the EPR phase keeps dark while the pores become green (Figure 17d).

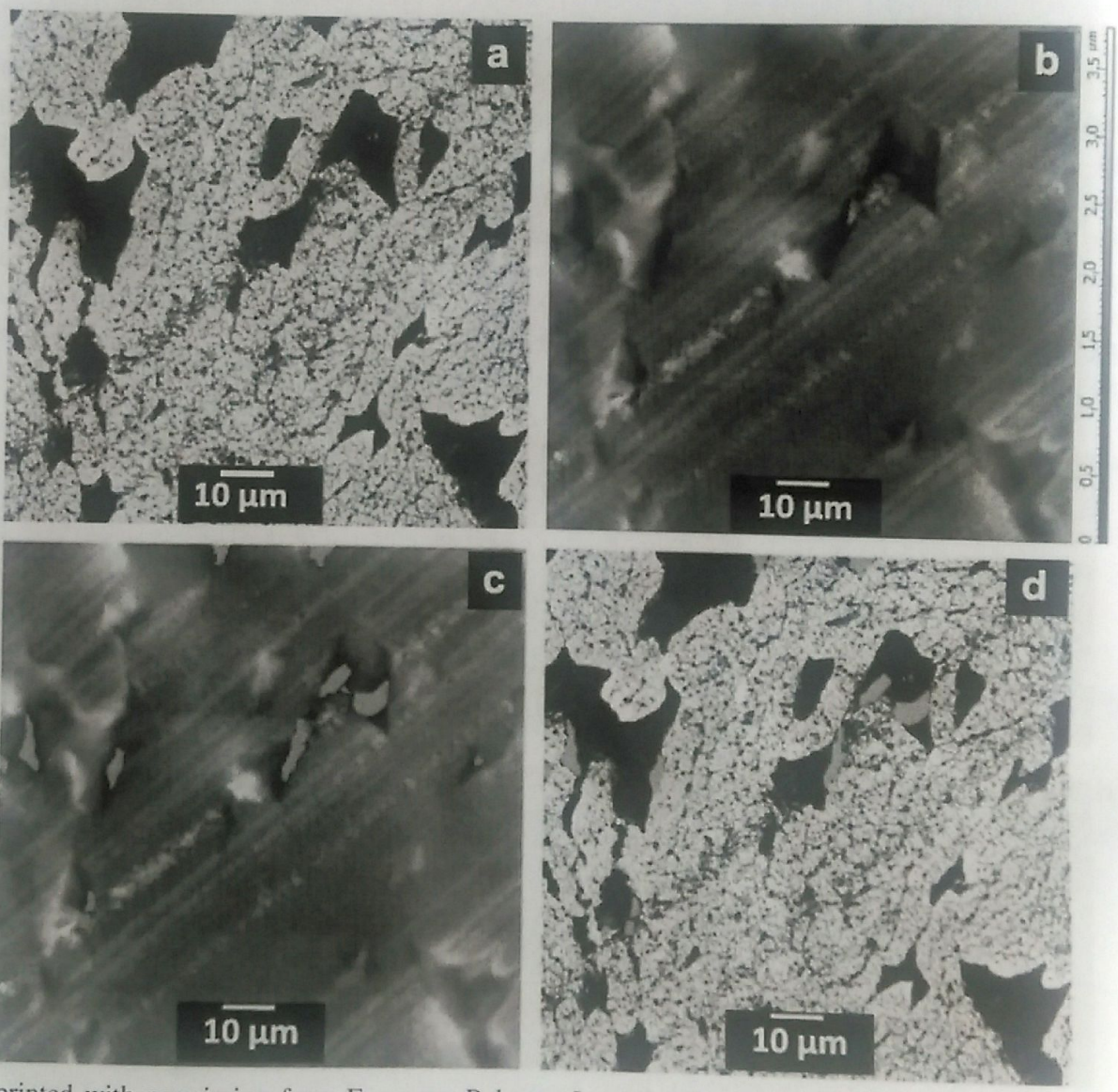

Reprinted with permission from European Polymer Journal 2013, 19, 3966-3976. Copyright (2013). Elsevier, Inc. [38].

Figure 17. (a) AFM phase image; (b) AFM topological image of the same area; (c) layer (mask) covering the pores in the topological image; (d) overlaid mask covering the pores (green) in AFM phase image. wEPR = 30%. Scanning parameters: generator frequency = 145.5 kHz, generator amplitude = 1.6 V, setpoint = 8.4 nA. (For interpretation of the references to color in this figure legend, the reader is referred to the web version of this article).

3. APPLICATION OF AFM

3.1. Effects of Temperature and Cultivar on Nanostructural Changes of Water-Soluble Pectin and Chelate-Soluble Pectin in Peaches

AFM was successfully applied to identify the heterogeneous structure of water-soluble pectin (WSP) and chelate-soluble pectin (CSP), including linear, branching, polymers or blocks [39]. The nanostructural changes of WSP and CSP of all cultivars were analyzed qualitatively and quantitatively by atomic force microscopy (AFM).

Figure 18 shows the AFM images of water-soluble pectin of 'Cangfangzaosheng' and 'Songsenzaosheng' peaches under cold storage. According to the AFM images, it can be indicted that the WSP molecules were aggregated, forming large polymers (p) or blocks (bl) from fresh peaches both of the two cultivars. Only a few of the WSP molecules form single linear chains (ls).

The size of the strands and polymers in 'Cangfangzaosheng' peaches gradually reduce during storage. The long single linear chains were detached while the small ones increased (compare Figure 18a and b). It is similar with the results observed when storage temperatures increased (compare Figure 18b–d).

Similar results were observed for 'Songsenzaosheng' peaches. With increasing of pectin esterase and polygalacturonase activities during fruit ripening, pectin substances in peaches were depolymerized and the pectin chain length was shortened. Then these changes were successfully imagined by AFM. Smaller aggregates of WSP molecules from fresh 'Songsenzaosheng' peaches were observed, comparing those from fresh 'Cangfangzaosheng' peaches. This cultivar difference may be the reason.

Figure 19 shows the nanostructural morphologies of chelate-soluble pectin (CSP) of peaches under cold storage. AFM images of CSP molecules were different from that of WSP. Single linear chains are the major nanostructure in the CSP molecules from peaches of both cultivars (Figure 19a). Only a few small aggregates were observed in fresh peaches while the size of single linear chains reduced with increased storage temperature during storage (Figure 19a).

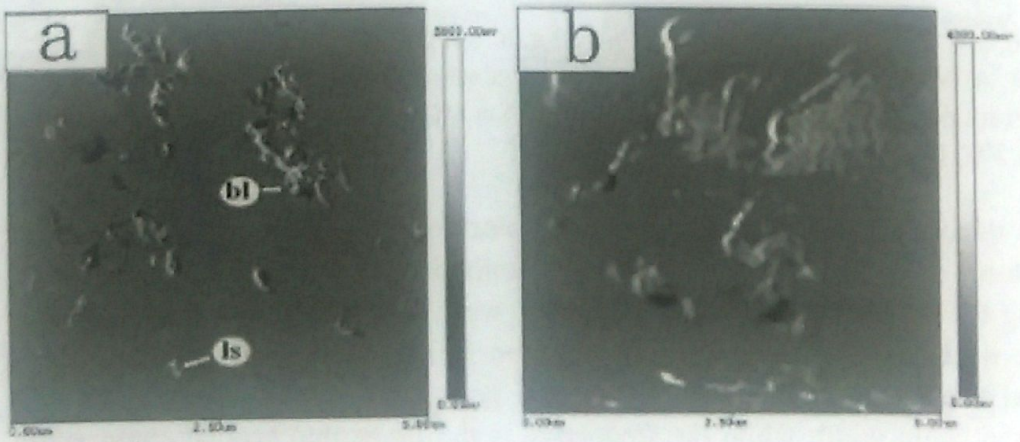

Figure 18. (Continued)

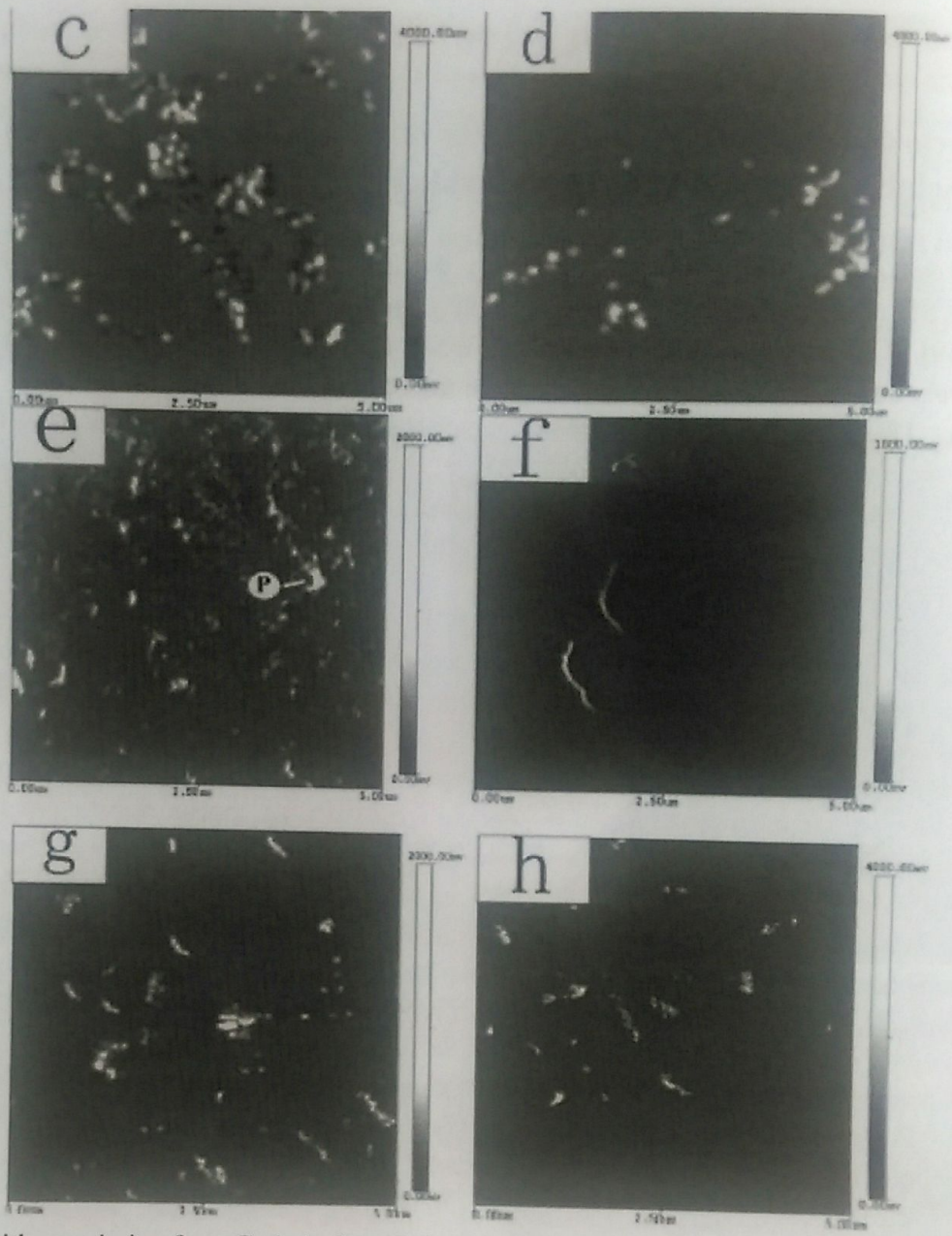

Reprinted with permission from Carbohydrate Polymers 2012, 87, 816-821. Copyright (2012), Elsevier, Inc. [39].

Note: a, b, c, d 'Cangfangzaosheng' peach; e, f, g, h 'Songsenzaosheng' peach.

Figure 18. AFM images of water-soluble pectin of peaches under cold storage. Scan area = 5 μm × 5 μm. (a) Fresh peaches; (b) day 26 at 2°C; (c) day 26 at 8°C; (d) day 26 at 15°C; (e) fresh peaches; (f) day 26 at 2°C; (g) day 26 at 8°C; (h) day 26 at 15°C.

The nanostructural changes of pectin molecules can also be analyzed quantitatively by atomic force microscopy (AFM). All the quantitative parameters of main chains of pectins, including the widths of linear single fractions were analyzed by section analysis of the AFM software while variance of the widths less than 1 nm was collected into the same groups for statistical analysis using SAS software. The peak width of chain half height was used to signify the chain width while the frequency is the times that special chain width occurred. Aggregated polymers and small linear chains which are unable to be visualized precisely by the software, were not applied for statistical analysis.

Tables 3 and 4 show the distributions of chain width and chain frequency of WSP and CSP molecules, respectively. During storage, frequency of WSP chains of smaller width was increased for both peach cultivars. More and more WSP chains of smaller width appear with the increasing of storage temperatures (Table 3).

Chain width distributions do not possess significant difference between the two cultivars. There is similarity between the trend of the width change of CSP molecules and that of WSP molecules. The change of WSP molecules is more significant than that of CSP molecules (Table 4).

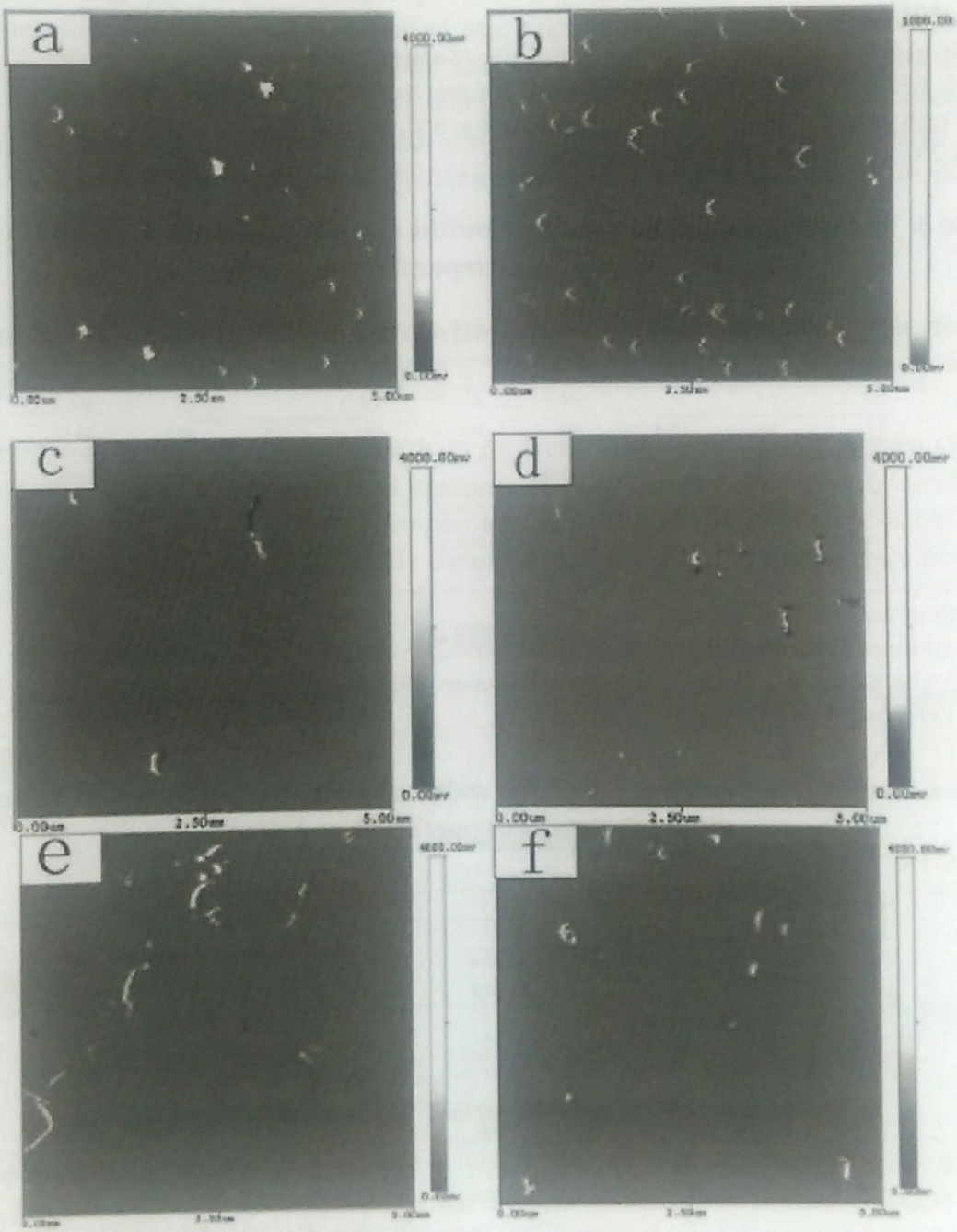

Figure 19. (Continued)

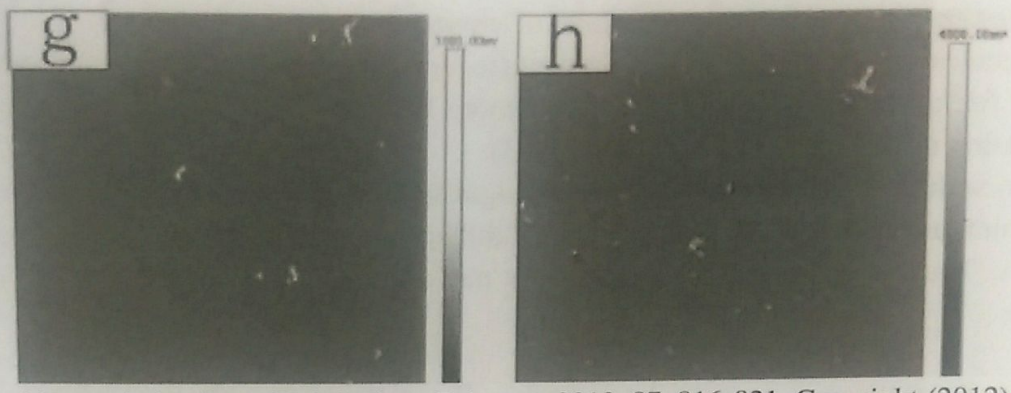

Reprinted with permission from Carbohydrate Polymers 2012, 87, 816-821. Copyright (2012), Elsevier, Inc. [39].

Note: a, b, c, d 'Cangfangzaosheng' peach; e, f, g, h 'Songsenzaosheng' peach.

Figure 19. AFM images of chelate-soluble pectin of peaches under cold storage. Scan area = 5 μm ×5 μm. (a) Fresh peaches; (b) day 18 at 2ºC; (c) day 18 at 8ºC; (d) day 18 at 15ºC; (e) fresh peaches; (f) day 18 at 2ºC; (g) day 18 at 8ºC; (h) day 18 at 15ºC.

Table 3. The water-soluble pectin chain widths and the frequency of peaches under different storage temperature and time

W (nm)[a]	Fq (*N* (%))[b]									
	Cangfangzaosheng					Songsenzaosheng				
	2°C			8°C	15°C	2°C			8°C	15°C
	0 d	26 d	41 d	26 d	26 d	0 d	26 d	41 d	26 d	26 d
54	-	1(2.5)	1(2.3)	-	-	-	-	-	-	-
72	-	2(5)	8(18.2)	1(14.3)	-	2(5)	-	2(5.9)	1(5)	3(11)
91	6(14)	8(20)	3(6.8)	3(42.9)	2(11.8)	3(7.5)	1(14.3)	8(23.5)	2(10)	3(11)
109	10(23.3)	14(35)	7(15.9)	1(14.3)	7(41.2)	12(30)	4(57.1)	20(58.8)	9(45)	9(33)
127	-	-	10(22.7)	2(28.6)	2(11.8)	-	-	-	1(5)	-
145	14(32.6)	12(30)	13(29.5)	-	5(29.4)	13(32.5)	2(28.6)	4(11.8)	7(35)	11(40.7)
181	9(20.9)	3(7.5)	2(4.5)	-	1(5.9)	10(25)	-	-	-	1(3.7)
217	4(9.3)	-	-	-	-	-	-	-	-	-

[a]The width of water-soluble pectin.

[b]Number of times particular chain widths were observed.

Reprinted with permission from Carbohydrate Polymers 2012, 87, 816-821. Copyright (2012), Elsevier, Inc. [39].

Table 4. The chelate-soluble pectin chain widths and the frequency of peaches under different storage temperature and time

W (nm)[a]	Fq (*N* (%))[b]									
	Cangfangzaosheng					Songsenzaosheng				
	2°C			8°C	15°C	2°C			8°C	15°C
	0 d	18 d	41 d	18 d	18 d	0 d	18 d	41 d	18 d	18 d
54	-	-	2(10.5)	-	-	-	-	-	-	3(5.2)
72	-	-	3(15.8)	-	-	-	-	-	1(4)	5(8.6)
91	3(17.6)	4(6.6)	5(26.3)	3(20)	3(12.5)	4(12.5)	1(5.6)	5(25)	-	6(10.3)
109	9(52.9)	10(16.4)	7(36.8)	4(26.7)	14(58.3)	11(34.4)	5(27.8)	4(20)	6(24)	21(36.2)
127	-	11(18)		2(13.3)	-	-	-	-	4(16)	5(8.6)
145	-	28(45.9)	1(5.3)	4(26.7)	7(29.2)	-	12(66.7)	9(45)	12(50)	14(24.1)
181	5(29.4)	8(13.1)	1(5.3)	2(13.3)	-	17(53.1)	-	2(10)	2(8.3)	4(6.9)

[a]The width of water-soluble pectin.

[b]Number of times particular chain widths were observed.

Reprinted with permission from Carbohydrate Polymers 2012, 87, 816-821. Copyright (2012), Elsevier, Inc. [39].

Basic units can be reflected by the chain widths of both WSP and CSP molecules from section analysis. For WSP molecules of 'Cangfangzaosheng' peach, 54, 72 and 91 nm were while 72, 91 and 109 nm were basic units for that of 'Songsenzaosheng' peach (Tables 3 and 4). The basic units of CSP molecules were 54, 72 and 91 nm both in 'Cangfangzaosheng' peach and 'Songsenzaosheng' peach.

The width of other types of chains can be composed by these basic units. For instance, 109 and 145 nm were approximately twice the size of 54 and 72 nm, respectively. Number of 217 nm was the sum of 54, 72 and 91 nm. Most of the wide values were the same for WSP molecules in both peach cultivars. In contrast, widths of 54 and 217 nm did not appear in 'Songsenzaosheng' peach but in 'Cangfangzaosheng' peach.

A schematic model of the degradation of peach pectin chains in width during cold storage was proposed based on the WSP and CSP chain widths described above (Figure 20). The frequency of smaller width values of WSP and CSP chains increased during cold storage. The long single linear chains were detached while the small ones increased. These finding suggests that both water-soluble and chelate-soluble pectin aggregates of peach gradually reduced during cold storage.

3.2. The Relation of Apple Texture with Cell Wall Nanostructure Studied Using an Atomic Force Microscope

The microstructure of nanostructure with different macroscopic may corresponds to the sensory qualities such as crispness and hardness of plant foods [40, 41]. Apple cell walls, which composed mostly of polysaccharides, are the main architecture responsible for the texture of parenchyma tissue and valuable component of one's daily diet as dietary fiber.

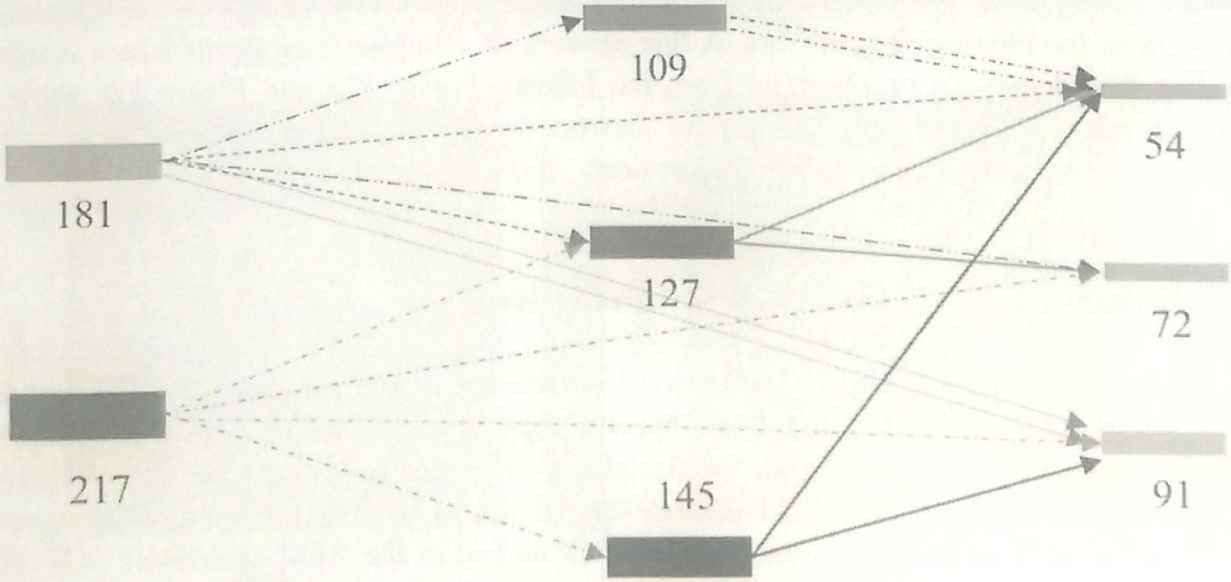

Reprinted with permission from Carbohydrate Polymers 2012, 87, 816-821. Copyright (2012), Elsevier, Inc. [39].

Note: Numbers indicate the width of pectin chains.

Figure 20. A schematic model of the degradation of peach pectin chains in width during cold storage.

The polysaccharides macromolecules are organized in a complex network supporting numerous functionalities and with architecture that have a significant influence on the whole parenchyma system, including mechanical properties. The mechanical properties of cell walls are controlled by the polysaccharide composition whereas the mechanical properties of parenchyma tissue are mainly depend on cell size, cell wall thickness and strength, turgor, and the extent of cell-to-cell adhesion.

AFM has been proved to be very useful in the comparison of nanostructures among different species for it can observe the molecular structure of a single macromolecule and cell wall assemblies. Cell wall material, roughness and network of cellulose microfibrils can be observed from AFM images and mean diameter of cellulose microfibrils can be estimated based on the AFM height topography [42, 43].

A successful study of the relation of apple texture with cell wall nanostructure was achieved by using atomic force microscopy [44]. Six apple cultivars were used to investigate the difference in terms of cellulose diameter, crystallinity, and pectin content. Figure 21 shows examples of the height AFM images of the cell wall material from investigated apple cultivars. From the images, cellulose microfibrils can be observed as the brighter and elongated objects. Image blurring and masking of the cellulose microfibrils maybe caused to the microfibrils which are embedded in a pectin/hemicellulose matrix.

After the root mean square roughness determined from the height images of cell wall material samples, it can be observed that the roughness of 'Honeycrisp' is significantly higher than other cultivars. While 'Ligol' and 'Mutsu' are slightly higher roughness, but not as high as 'Honeycrisp' whereas 'Cortland', 'Jonagold' and 'Rubin' possessed the smallest roughness according to the height AFM images.

In general, it is difficult to estimate the diameter of cellulose microfibrils from the height image of cell wall material samples due to the presence of the matrix polysaccharides. Therefore, in order to reveal the cellulose network, the pectin and hemicellulose matrix should be removed. Figure 22 shows examples of the height AFM images of the cellulosic network of the investigated cultivars. A fine network of cellulose microfibrils which is more or less disordered can be observed from the images. Figure 22a and Figure 22c show a random microfibril orientation within the network whereas the other cultivars show some preferences in the direction of fibril arrangement.

3.3. Galectin 3 and B-Galactobiose Interactions

Gal3, which is widely found from lower invertebrates to mammals, is the most versatile galactose-binding lectin [45, 46]. Force spectroscopy was a useful tool to investigate the interaction between the disaccharide ß-galactobiose and galectin-3 (Gal3). In order to probe β-galactobiose interactions, the carbohydrate-coated silica beads were often stressed against Gal3-coated glass surfaces following attaching to the end of the AFM cantilevers [47]. The AFM tip were ramped towards the sample surface under buffer solution and then away from the surface at a controlled speed to finish the measurements.

Figure 23 shows the force versus galactobiose-Gal3 rupture events. From the retract part of the force curves, the magnitude of the detachment force can be investigate together with

the loading rate. AFM which allows plotting the force data directly against time will provide higher accuracy than the 'effective spring constant' method.

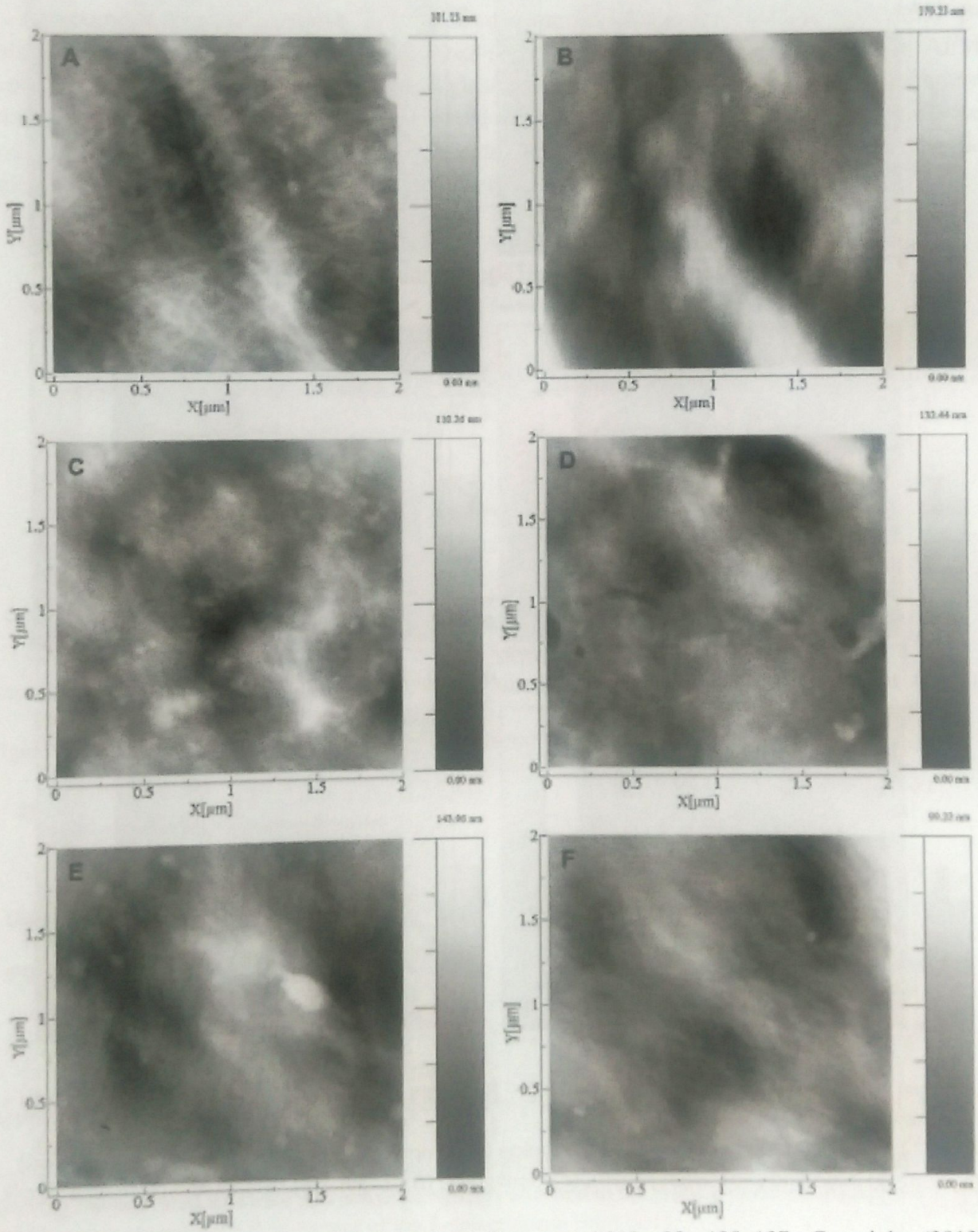

Reprinted with permission from Carbohydrate Polymers 2013, 92, 128–137. Copyright (2013), Elsevier, Inc. [44].

Figure 21. The height images from atomic force microscope (AFM) in tapping mode revealing cell wall material (CWM) nanostructures for: (a) 'Cortland', (b) 'Honeycrisp', (c)'Jonagold', (d) 'Ligol', (e) 'Mutsu' and (f) 'Rubin' apple cultivars.

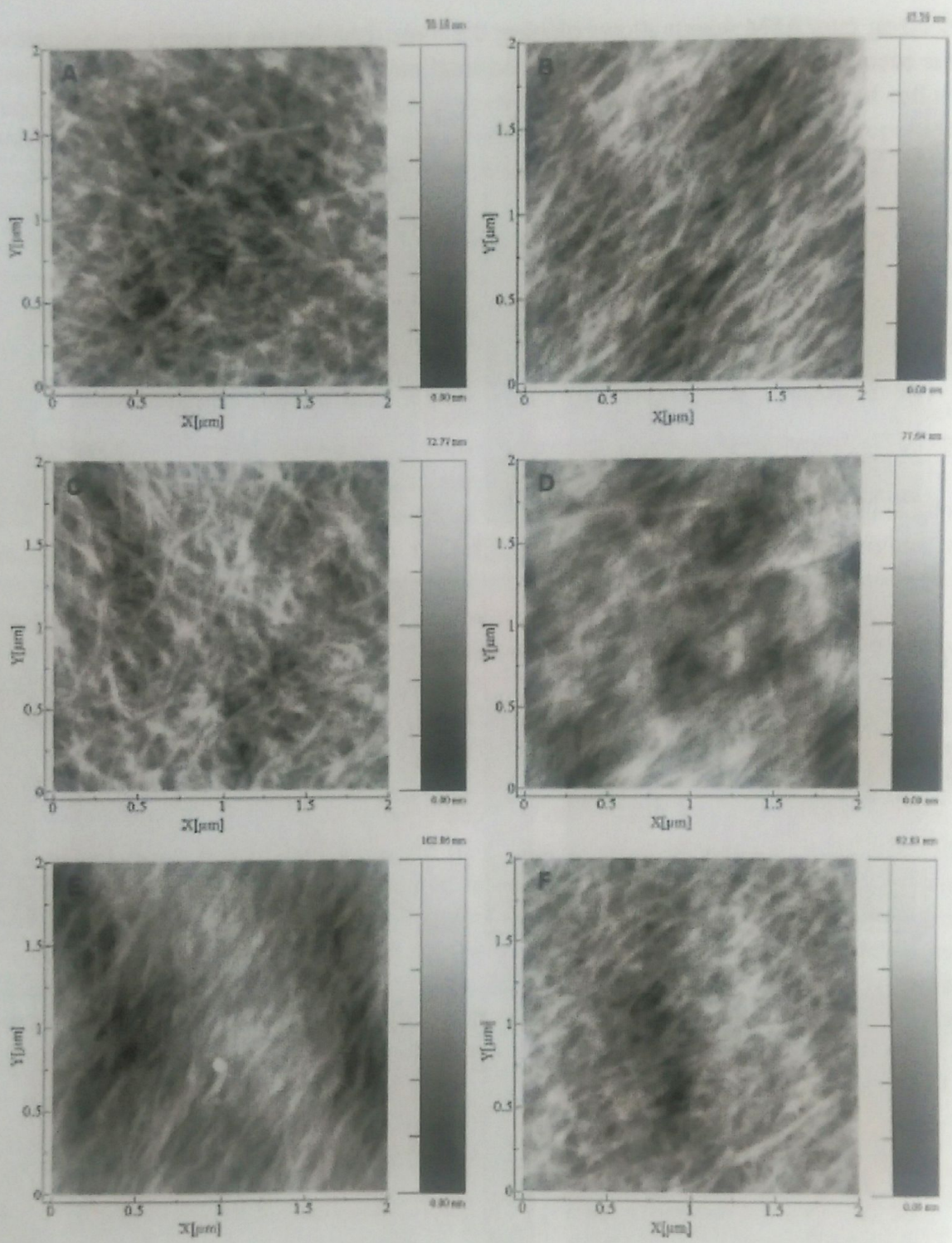

Reprinted with permission from Carbohydrate Polymers 2013, 92, 128–137. Copyright (2013), Elsevier, Inc. [44].

Figure 22. The height images from AFM in tapping mode presenting cellulosic nanostructures of cell walls for: (a) 'Cortland', (b) 'Honeycrisp', (c) 'Jonagold', (d) 'Ligol', (e) 'Mutsu'and (f) 'Rubin' apple cultivars.

Of the two the latter perform the analysis based on the slope of force versus distance curve at the rupture point with higher pulling speeds which are edited in the instrument software. The regression slope of those points following a linear pattern is corresponding to the loading rate at bond rupture. After setting the threshold for the magnitude of the rupture

force based on the noise, determination of the magnitude was performed by quantifying the difference between force value at the rupture point and a linear fit in the off region of the data. Potential specific binding of β-galactobiose to Gal3 can be investigated by force spectroscopy. Figure 24 shows schematic diagram on determination of Gal3 and β-galactobiose interactions. The β-galactobiose-activated spheres were attached to the AFM cantilever while Gal3 was attached to the glass substrate via PEG spacer molecules (Figure 24a). The example curves in Figure 24b reveal evidence of a binding between β-galactobiose and Gal3. The flexible PEG spacer has extension followed by the breakage of the β-galactobiose–Gal3 linkage and hence the retract curve appears in Figure 24b.

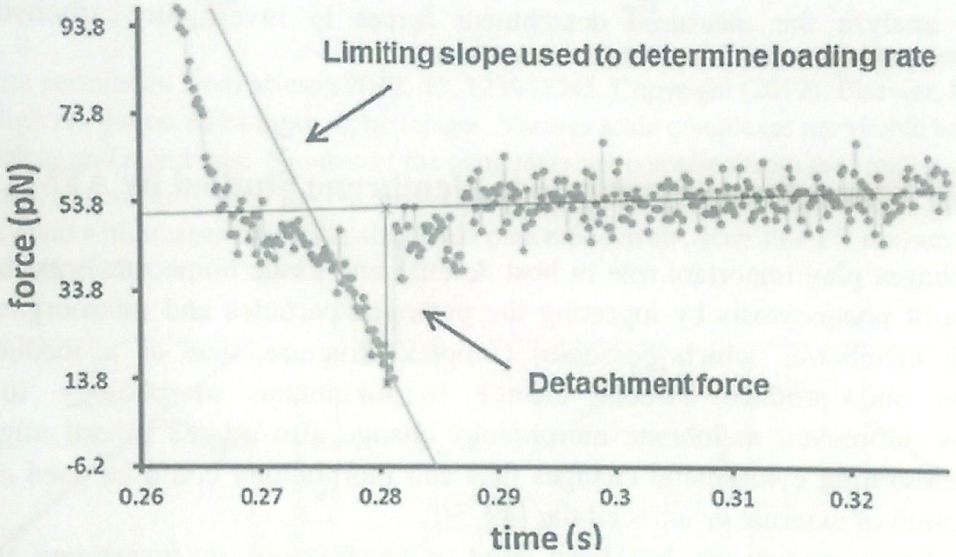

Reprinted with permission from Carbohydrate Polymers 2013, 92, 529–533. Copyright (2013), Elsevier, Inc. [47].

Figure 23. Analysis of force versus time data for galactobiose–Gal3 rupture events.

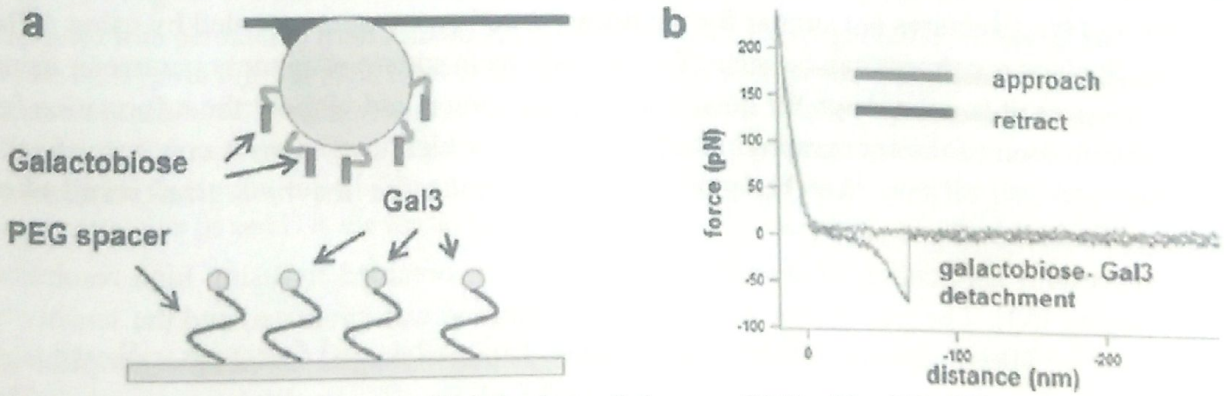

Reprinted with permission from Carbohydrate Polymers 2013, 92, 529–533. Copyright (2013), Elsevier, Inc. [47].

Figure 24. Force spectroscopy studies of Gal3 and β-galactobiose interactions. (a) Schematic diagram showing the activated substrate and activated spheres attached to the AFM cantilever. (b) Approach and retract curves showing the detachment of the β-galactobiose from Gal3.

With allowing the molecules geometrical freedom, binding of Gal3 to β-galactobiose happened with the presence of the PEG spacer. So, molecular weight can be one way to distinguish between specific and non-specific binding events.

When there is non-specific interactions between the carbohydrate and protein, the retract curve will show up at this point of contact. Contrarily, if interactions between the carbohydrate and protein are specific binding events, a characteristic non-linear peak will appear in the curve due to stretching of the PEG. Interaction of β-galactobiose with Gal3 are clearly observed in Figure 24b showing both hallmarks of specific binding.

When carrying out AFM experiments, there are always a range of detachment forces. The modal value of the measured detachment forces may reveal which interaction there is between β-galactobiose and Gal3. The measured detachment force varies with loading rates. At very slow loading rates, the measured detachment force will be zero because that the lectin will have sufficient time to dissociate interaction with the carbohydrate ligand. So, it is feasible to analyze the measured detachment forces to investigate carbohydrate–lectin interaction.

3.4. Fractal Properties of Macrophage Membrane Studied by AFM

Macrophages play important role in host defense and tissue homeostasis as they possess the function of phagocytosis by ingesting the pathogen particles and microorganisms [48]. Macrophage membrane, which possesses complex structure, acts as a mediator of the phagocytosis and produce evident change in membrane morphology to continue phagocytosis. Moreover, membrane morphology change also related to cell migration and proteins orchestrating cytoskeletal changes thus cell morphology could be used as a tool to sense the stimuli of external or intracellular [49, 50].

Atomic force microscope has been used as useful tool to investigate the surface morphology of macrophage by recognizing the complicated structure of macrophage membrane through the images. The details that cell membrane structures span three orders of magnitude scales corresponding to the features with sizes ranging from nanometers to microns and the structures are similar for the different cell types were revealed by using AFM [51, 52]. Surface roughness can be quantified by root mean square roughness parameter using AFM. However, it is not enough for quantitative investigation and without the information for spatial distribution of the topography. Fractal geometry, which is used with concepts of self-similarity and self-affinity, has been proposed to characterize the biological surfaces of structures for cells.

A successful application of fractal analysis has been obtained by using high resolution AFM imaging [53]. The fractal dimension of cell membrane was evaluated and the sensitivity of fractal dimension value to sub-micron changes in macrophages membrane morphology was determined.

Figure 25 shows high resolution AFM topography images of macrophages. It reveals that large complexes are built from small complexes which in turn are built from smaller so that some self-similarity can be recognized already by visual inspection of images.

The typical log-log graphs illustrating calculation of fractal dimension are presented in Figure 26. The fractal dimension value of macrophages including treated and untreated was calculated by using three different methods.

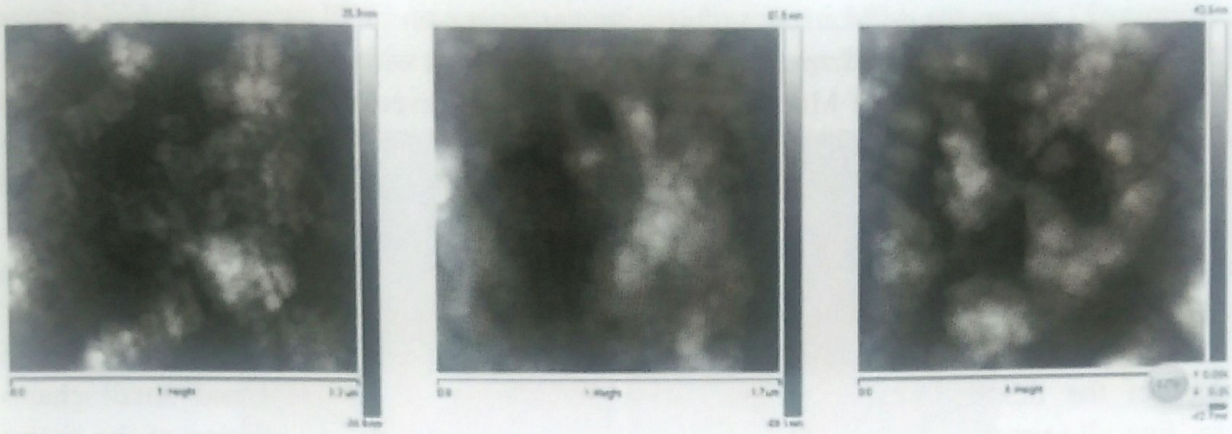

a b c

Reprinted with permission from Micron 2012, 43, 1239–1245. Copyright (2012), Elsevier, Inc. [53].
Figure 25. High resolution AFM topography images. Various scale complexes are visible both in the region of nucleus and membrane. Number of the complexes are compiled from the smaller clusters. (A) Untreated cells, (B) colchicine (10 μM) treated cells, and (C) taxol (10 μM) treated cells. Fractal analysis was done with images of similar size PeakForce mode in air. Scan size 1.7 μm, scan rate 1 Hz, pixel number 512×512.

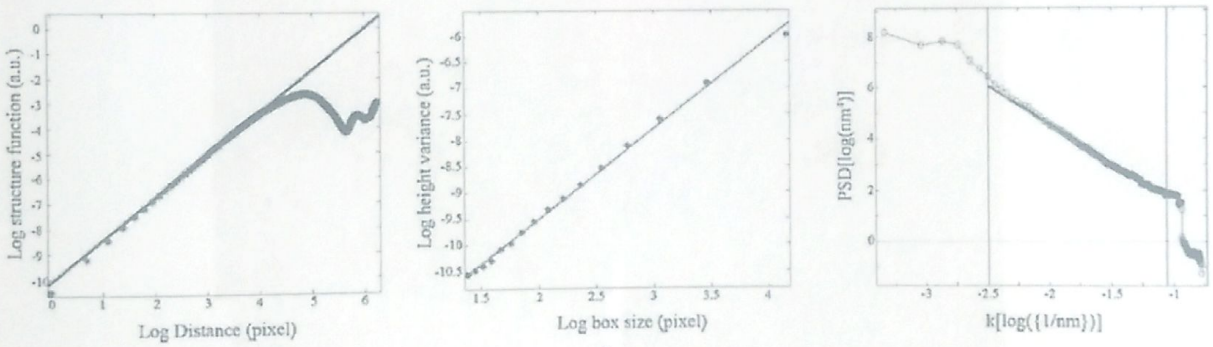

a b c

Reprinted with permission from Micron 2012, 43, 1239–1245. Copyright (2012), Elsevier, Inc. [53].
Figure 26. Typical log–log plots illustrating calculation of fractal dimension by different methods. (A) Structure function, (B) height variance, and (C) power spectrum. Circles represent experimental data and straight line represents linear regression fit. The slope of the linear regression line is directly related to the fractal dimension value by equation $K = 2(3-D)$, where K is the slope of the line obtained from linear regression fit and D is the fractal dimension.

3.5. Studies on the Mucoadhesion Mechanism of Pectin by Atomic Force Microscopy and Mucin-Particle Method

Since Duchene Touchard, and Peppas proposed the mucoadhesive mechanism in 1988 [54]. Atomic force microscopy (AFM) has been used to probe the interaction between mucin and pectin with different chemical characteristics. The structure and state of pectin adsorbed on mucin molecules was observed by the AFM in a recent experiment [55]. The association of the pectin and mucin in water medium might be due to the formation of H-bond. AFM imaging can show the procedure of the H-bond formation.

Figure 27 shows the AFM images of porcine gastric mucin in DI water. The AFM image of Mucin particles in acid medium revealed aggregated chains with a large size.

However, AFM image of Mucin particles in DI water revealed a particle structure with the aggregation of small particles which were smaller than that in 0.1 N HCl (Figure 27). This was probably due to the formation of gel on porcine stomach mucin at low pH but dispersed at higher pH. The electrostatic repulsion was smaller relatively in low pH and dilute solutions. So it was easier to form the aggregated chains of polymers. The dried mucin possesses numerous H-bonding groups and hence it can be dispersed in aqueous medium.

Figure 28 shows the morphology of mixture of a pectin and mucin in DI water. The AFM image of the mixture in acid medium revealed some large particles and small chains spreading all over the image, without cross-linking. In contrast, the association of the chains was clearly observed in the mixture in DI water (Figure 28). The possible explanation for these interactions is that the hydrophobic interaction between pectin and mucin may establish for bond formation in DI water. Meanwhile, the uncharged segments in pectin molecules could associate with mucin due to the formation of H-bond.

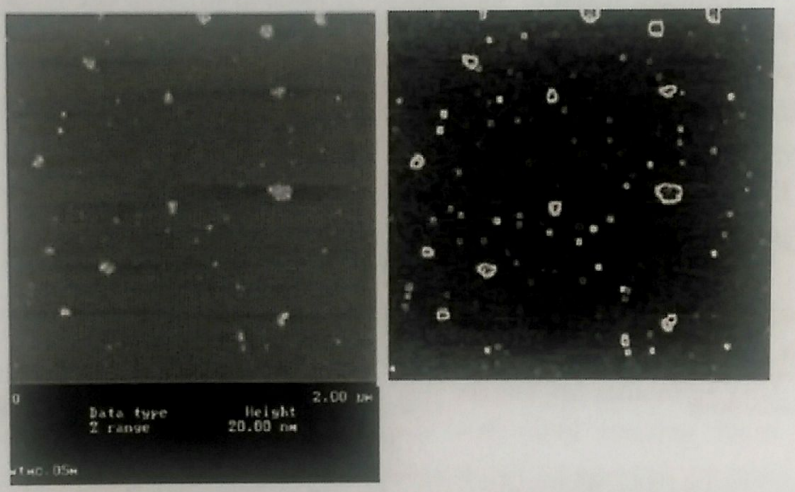

a

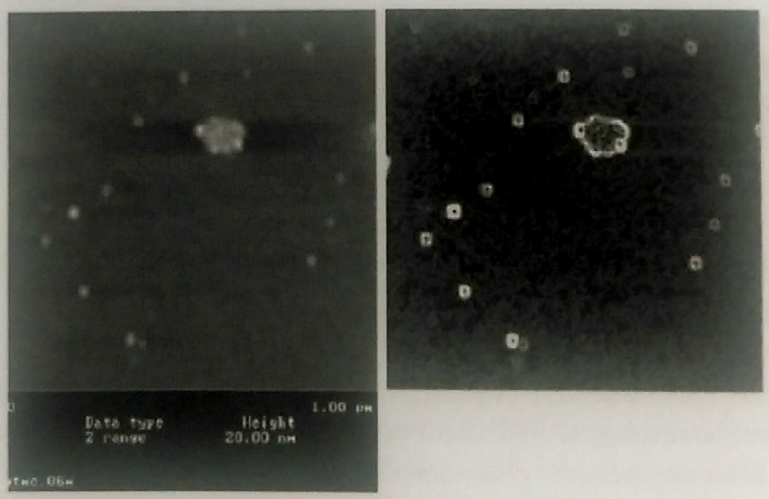

b

Reprinted with permission from Carbohydrate Polymers 2010, 79, 54–59. Copyright (2010), Elsevier, Inc. [55].

Figure 27. Topographical (left) and equivalent processed (right) images from AFM of mucin in DI water; (a) image size 2.0 × 2.0 μm^2 and (b) image size 1.0 × 1.0 μm^2.

Because pectin CU020 possesses amide groups and carboxyl groups, the H-bond formation may be stronger than that of CU701 which has only carboxyl groups (Figure 28).

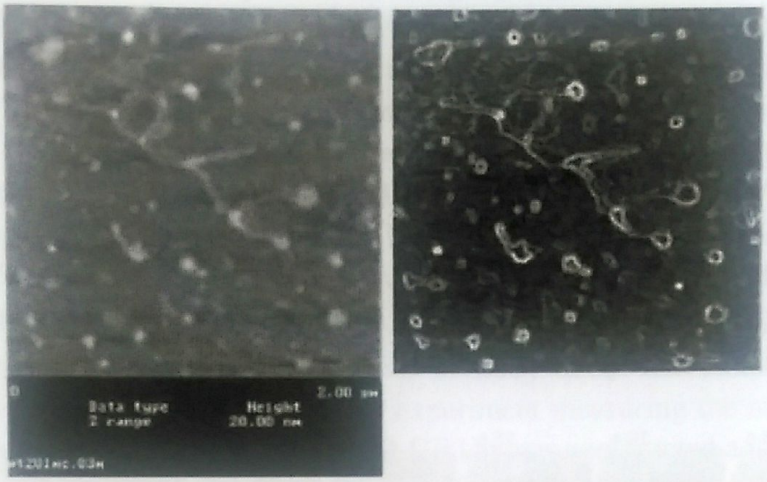

a

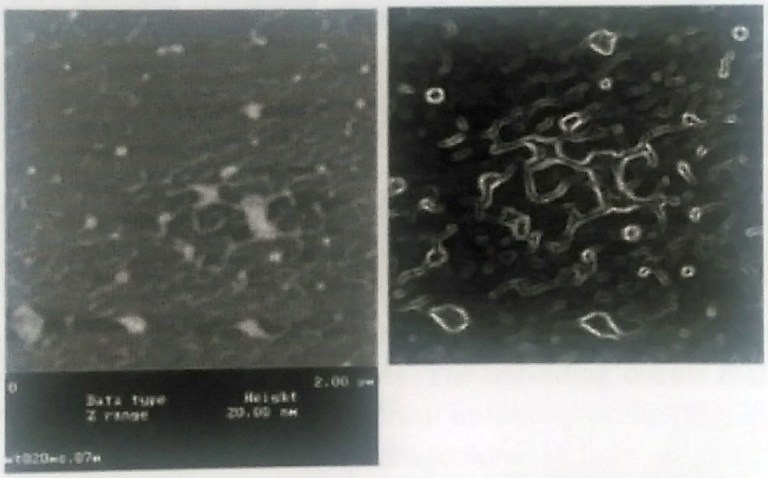

b

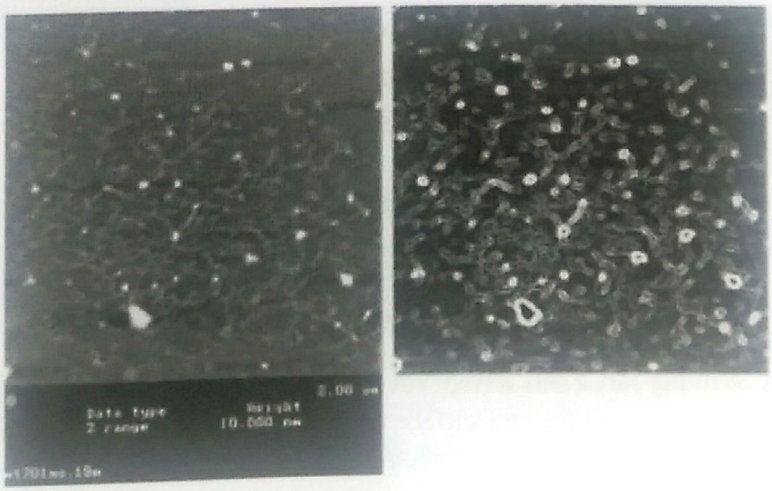

c

Reprinted with permission from Carbohydrate Polymers 2010, 79, 54–59. Copyright (2010), Elsevier, Inc. [55].

Figure 28. Topographical (left) and equivalent processed (right) images from AFM of the mixture between pectin and mucin in DI water, (a) CU201, (b) CU020 and (c) CU701. Image size is 2.0 × 2.0 μm^2.

3.6. Dynamics Analysis of Living Hela Cell Surface with High-Speed AFM

The dynamics of the cell membrane was regulated by the coordinated polymerization of actin filaments at the periphery of the cell [56]. This coordinated polymerization also organizes numerous cellular events including morphogenesis, cell migration, phagocytosis, and endocytosis. However, it is difficult to observe the dynamics of cell morphology with sufficient time and spatial resolution when using only fluorescence approaches. An implementation of high-speed AFM coupled with an optical fluorescence microscope was developed to capture the dynamic behavior of the living HeLa cell surface [11]. Figure 29 shows dynamics of living HeLa cell surface revealed by high-speed AFM. A series of images AFM images recorded at a scan rate of 0.2 fps showed dynamic characters of the cell surface reflecting the motion of filopodia (Figure 29a).

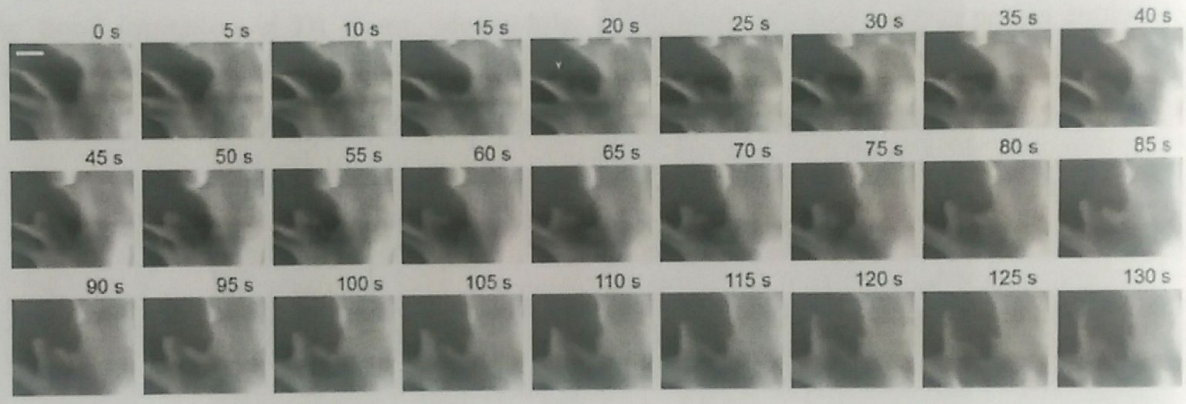

a

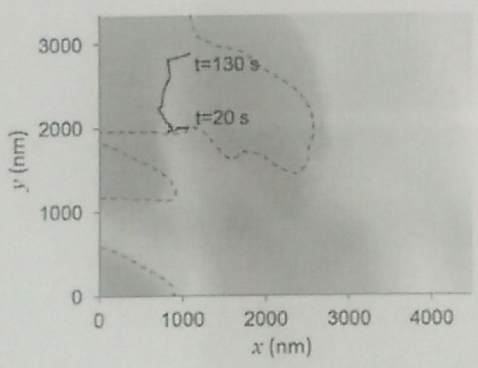

b

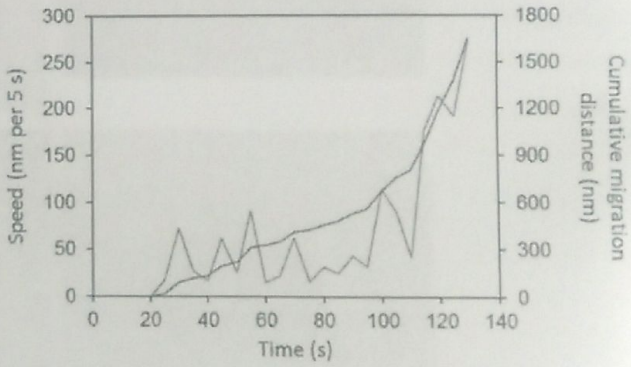

c

Reprinted with permission from Scientific Reports 2013, 3, 2131. Copyright (2013), Nature publishing group, Inc. [11].

Figure 29. Dynamics of living HeLa cell surface revealed by high-speed AFM. (a) High-speed AFM images showed dynamic features of the cell surface reflecting the motion of filopodia. Images were recorded at a scan rate of 0.2 fps. Image size: 4480 nm × 3360 nm. Scale bar: 1 mm. For the complete movie, see Supplementary Movie S1 online. (b) Trajectory of the tip of the protrusion (yellow arrowhead in the image at 20 s) in 23 sequential images (20–130 s) was overlaid on the sepia colored image at 130 s (blue line). Dashed gray lines represent the shape of the cell at 20 s. (c) Changes of the elongation speed of the protrusion (red) and the cumulative migration distance (blue). The elongation speed at each time point was determined by measuring the distance between the tip of the protrusion in the current frame and that in the previous frame.

Protrusions of filamentous structures at the edge of HeLa cells were clearly exhibited in the images. By plotting the tip of the protrusions, the elongation event was quantified at each time point (Figure 29b and 29c). As shown in Figure 4c, the protrusion generated at rates between 16 and 112 nm per 5 s from 20 s to 110 s. From 110 s, there is accelerated elongation. The protrusion generated at rates of about 272 nm per 5 s at 130 s (Figure 29c).

3.7. Determine the Mechanical Unfolding of the Polyprotein (Zn-pfRD-GB1)n Via Single-Molecule AFM

In order to distinguish single-molecule unfolding events from those of nonspecific interactions, polyproteins were frequently used in study about the mechanical stability of proteins by using single-molecule AFM. In an experiment measuring the mechanical stability of Zn-thiolate bonds, the polyprotein (Zn-pfRD-GB1)n was constructed and the GB1 domains serve as a fingerprint to identify single-molecule unfolding events of Zn-pfRD [57].

Figure 30 shows the schematics of polyprotein (Zn-pfRDGB1) n stretching between cantilever and solid substrate, as well as typical force extension curves for the unfolding of the polyprotein (Zn-pfRD-GB1)n.

The curves show typical sawtooth-like patterns (Figure 30, dotted lines) while every individual force peak in the curve corresponds to the mechanical unfolding of an individual domain in the polyprotein. The fully extended polyprotein chain can stretch and detach from either the AFM tip or the glass coverslip. The stretching and subsequent detachment corresponds to the last peak in the AFM curves.

The unfolding force peaks show in Figure 30B revealed two populations of unfolding events with different contour length increments. The unfolding events that exhibit a DLc of ~18 nm (colored in black) are from the mechanical unfolding of the fingerprint GB1 domains (Figure 30 A). The events with a DLc of ~13 nm (colored in light color and indicated by * in Figure 3B) corresponds to the unfolding of Zn-RD (Figure 30A).

CONCLUSION

AFM has been applied to characterize molecular structures and molecular interactions. It has successfully provided qualitative and quantitative information of food macromolecule structures and molecular interactions.

AFM results modified our previous understanding of pectin molecular structures, furthered the knowledge about the relation of fruit texture with cell wall nanostructure, and elucidated the mucoadhesion mechanism of pectin.

To date, this kind of information is hardly achieved by other techniques except AFM, although AFM has its own limitations, which is that there is no standard protocol for various study objects. Therefore, it is urgent to develop standard methodologies and procedures for better applying this technology in different areas.

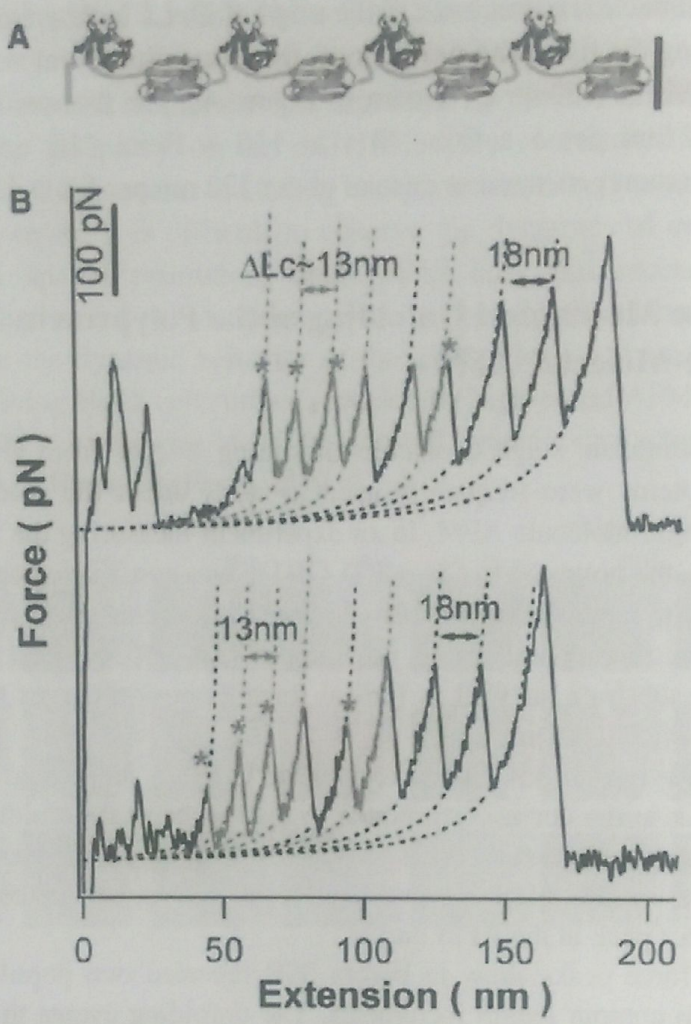

Reprinted with permission from Biophysical Journal 2011, 101, 1467-1473. Copyright (2011), Elsevier, Inc. [57].

Figure 30. Mechanical unfolding of the polyprotein $(Zn\text{-}pfRD\text{-}GB1)_n$ via single-molecule AFM. (A) Schematics of polyprotein $(Zn\text{-}pfRDGB1)_n$ stretching between cantilever and solid substrate. Zn-pfRD and GB1 are colored in dark and light colors, respectively. (B) Typical force extension curves for the unfolding of the polyprotein $(Zn\text{-}pfRD\text{-}GB1)_n$ in which Zn-thiolate bonds are ruptured. The curves show characteristic sawtooth-like patterns. The unfolding force peaks can be fitted well using the worm-like chain model of polymer elasticity (dotted lines). Two populations of unfolding events are observed with different contour length increments. The unfolding events corresponding to a ΔLc of ~18 nm (colored in black) are from the mechanical unfolding of the fingerprint GB1 domains. Thus, the other unfolding events of ΔLc ~13 nm (colored in light color and indicated by *) can be attributed to the unfolding of Zn-RD, which is triggered by the rupture of Zn-thiolate bonds.

ACKNOWLEDGMENTS

H.Y. thanks the start-up grant (R-143-000-561-133), teaching enhancement grant (C-143-000-041-001) and LIFT project (C-143-100-002-511) provided by the National University of Singapore for supporting this work. Projects 31371851, 31071617 and 31200801 supported by NSFC also contributed to this research.

REFERENCES

[1] Yang, H., Wang, Y., Lai, S., An, H., Li, Y., Chen, F. (2007). Application of atomic force microscopy as a nanotechnology tool in food science. *J. Food Sci.* 72, R65-75.

[2] Binnig, G., Quate, C. F., Gerber, C. (1986) . Atomic force microscope. *Phys. Rev. Lett.* 56, 930–933.

[3] Hansma, P. K., Elings, V. B., Marti, O., Bracker, C. E. (1988). Scanning tunneling microscopy and atomic force microscopy: application to biology and technology. *Science* 242, 209–216.

[4] Whited, A. M., Park, P. S. (2014). Atomic force microscopy: A multifaceted tool to study membrane proteins and their interactions with ligands. *Biochim. Biophys. Acta* 1838 (1), 56-68.

[5] Gerber, C., Lang, H. P. (2006). How the doors to the nanoworld were opened. *Nat. Nanotechnol.* 1, 3–5.

[6] Parot, P., Dufrene, Y. F., Hinterdorfer, P., Grimellec, C. L., Navajas, D., Pellequer, J. L., Scheuring, S. (2007). Past, present and future of atomic force microscopy in life sciences and medicine. *J. Mol. Recognit.* 20, 418–431.

[7] Noy, A. (2011). Force spectroscopy 101: how to design, perform, and analyze an AFM-based single molecule force spectroscopy experiment. *Curr. Opin. Chem. Biol.* 15(5): 710-718.

[8] Fechner, P., Boudier, T., Mangenot, S., Jaroslawski, S., Sturgis, J. N., Scheuring, S. (2009). Scheuring, Structural information, resolution, and noise in high-resolution atomic force microscopy topographs. *Biophys. J.* 96, 3822–3831.

[9] Pietrasanta, L. I., Schaper, A., Jovin, T. M. (1994). Imaging subcellular structures of rat mammary carcinoma cells by scanning force microscopy. *J. Cell Sci.* 107(Pt 9), 2427–2437.

[10] Tamura, K., Mizutani, T., Haga, H., Kawabata, K. (2010). Nano-mechanical properties of living cells expressing constitutively active RhoA effectors. *Biochem. Biophys. Res. Commun.* 403, 363–367.

[11] Suzuki, Y., Sakai, N., Yoshida, A., Uekusa, Y., Yagi, A., Imaoka, Y., Ito, S., Karaki, K., Takeyasu, K. (2013). High-speed atomic force microscopy combined with inverted optical microscopy for studying cellular events. *Sci. Rep.* 3, 2131.

[12] Webber, G. B., Edwards, S. A., Stevens, G. W., Grieser, F., Dagastine, R. R., Chan, D. Y. C. (2008). Measurementsof dynamic forces between drops with the AFM: Novel considerations in comparisons between experiment and theory. *Soft Matter* 4, 1270–1278.

[13] Elsabee, M. Z., Abdou, E. S. (2013). Chitosan based edible films and coatings: A review. *Mater. Sci. Eng. C Mater. Biol. Appl.* 33(4), 1819-1841.

[14] Jayakumar, R., Menon, D., Manzoor, K., Nair, S. V., Tamura, H. (2010). Biomedical applications of chitin and chitosan based nanomaterials—A short review. *Carbohydr. Polym.* 82(2), 227-232.

[15] Abu-Lail, N. I., Camesano, T. A. (2003). Polysaccharide properties probed with atomic force microscopy. *J. Microsc.* 212, 217–238.

[16] Kocun, M., Grandbois, M., Cuccia, L. A. (2011). Single molecule atomic force microscopy and force spectroscopy of chitosan. *Colloids Surf. B Biointerfaces* 82(2), 470-476.

[17] Neuman, K. C., Nagy, A. (2008). Single-molecule force spectroscopy: optical tweezers, magnetic tweezers and atomic force microscopy. *Nat. Methods* 5(6), 491-505.

[18] Hinterdorfer, P., Dufrêne, Y. F. (2006). Detection and localization of single molecular recognition events using atomic force microscopy. *Nat. Methods* 3, 347–355.

[19] Reising, A., Yao, C., Storey, D., Webster, T. J. (2008). Thomas, Greater osteoblast long-term functionson ionic plasma deposited nanostructured orthopedic implant coatings. *J. Biomed. Mater. Res.* A 87(1), 78–83.

[20] Quesada, M. A., Blanco-Portales, R., Posé, S., García-Gago, J. A., Jiménez-Bermúdez, S., Muñoz-Serrano, A., Caballero, J. L., Pliego-Alfaro, F., Mercado, J. A., Muñoz-Blanco, J. (2009). Antisense down-regulation of the FaPG1 gene reveals an unexpected central role for polygalacturonase in strawberry fruit softening. *Plant Physiol.* 150, 1022–1032.

[21] Santiago-Doménech, N., Jiménez-Bemúdez, S., Matas, A. J., Rose, J. K., Muñoz-Blanco, J., Mercado, J. A., Quesada, M. A. (2008). Antisense inhibition of a pectate lyase gene supports a role for pectin depolymerization in strawberry fruit softening. *J. Exp. Bot.* 59, 2769–2779.

[22] Adams, E. L., Kroon, P. A., Williamson, G., Morris, V. J. (2003). Characterisation of heterogeneous arabinoxylans by direct imaging of individual molecules by atomic force microscopy. *Carbohydr. Res.* 338, 771–780.

[23] Poséa, S., Kirbyc, A. R., Mercadob, J. A., Morrisc, V. J., Quesadaa, M. A. (2012). Structural characterization of cell wall pectin fractions in ripe strawberry fruits using AFM. *Carbohydr. Polym.* 88, 882-890.

[24] Morris, V. J., Gromer, A., Kirby, A. R., Bongaerts, R. J. M., Gunning, A. P. (2011). Using AFM and force spectroscopy to determine pectin structure and (bio) functionality. *Food Hydrocoll.* 25, 230-237.

[25] Liu, S., Wang, Y. (2010). Application of AFM in microbiology: a review. *Scanning* 32, 61–73.

[26] McKee, C. T., Raghunathan, V. K., Nealey, P. F., Russell, P., Murphy, C. J. (2011). Topographic modulation of the orientation and shape of cell nuclei and their influence on the measured elastic modulus of epithelial cells. *Biophys. J.* 101, 2139–2146.

[27] Gaboriaud, F., Parcha, B. S., Gee, M. L., Holden, J. A., Strugnell, R. A. (2008). Spatially resolved force spectroscopy of bacterial surfaces using force–volume imaging. *Colloids Surf. B Biointerfaces* 62, 206–213.

[28] Chopineta, L., Formosaa, C., Rolsb, M. P., Duvale, R. E., Daguea, E. (2013). Imaging living cells surface and quantifying its properties at high resolutionusing AFM in QI™ mode. *Micron* 48, 26-33.

[29] Smela, E., Mattes, B. R. (2005). Polyaniline actuators. Part 2. PANI(AMPS) in methanesulfonic acid. *Synth. Met.* 151, 43–48.

[30] Daoud, W. A., Xin, J. H., Szeto, Y. S. (2005). Polyethylenedioxythiophene coatings for humidity, temperature and strain sensing polyamide fibers. *Sens. Actuat. B* 109, 329–333.

[31] Smela, E., Lu, W., Mattes, B. R. (2005). Polyaniline actuators. Part 1. PANI(AMPS) in HCl. *Synth. Met.* 151, 25–42.

[32] Abidian, M. R., Kim, D. H., Martin, D. C. (2006). Conducting-polymer nanotubes for controlled drug release. *Adv. Mater.* 18, 405–409.

[33] Long, Y. Z., Li, M. M., Gu, C., Wan, M., Duvail, J. L., Liu, Z., et al. (2011). Physical properties and applications of conducting polymer nanotubes and nanofibers. *Prog. Polym. Sci.* 36, 1415–1442.

[34] Passeri, D., Biagioni, A., Rossi, M., Tamburri, E., Terranova, M. L. (2013). Characterization of polyaniline–detonation nanodiamond nanocomposite fibers by atomic force microscopy based techniques. *Eur. Polym. J.* 49, 991-998.

[35] Tetard, L., Passian, A., Farahi, R. H., Kalluri, U. C., Davison, B. H., Thundat, T. (2010). Spectroscopy and atomic force microscopy of biomass. *Ultramicroscopy* 110 (6), 701-707.

[36] Tetard, L., Passian, A., Thundat, T. New modes for subsurface atomic force microscopy. (2009). *Nat. Nanotechnol.* 5(2), 105-109.

[37] Olivares, M. L., Passeggi, Jr M. C. G., Ferrón, J., Zorrilla, S. E., Rubiolo, A. C. (2010). Study of milk/k-carrageenan mixtures by atomic force microscopy. *Food Hydrocoll.* 24, 776-782.

[38] Klára Smolná, Tomáš Gregor, Juraj Kosek. (2013). Morphological analysis of high-impact polypropylene using X-ray microCT and AFM. *Eur. Polym. J.* 49(12), 3966-3976.

[39] Zhang, L., Chen, F., Yang, H., Ye, X., Sun, X., Liu, D., Yang, B., An, H., Deng, Y. (2012). Effects of temperature and cultivar on nanostructural changes of water-soluble pectin and chelate-soluble pectin in peaches. *Carbohydr. Polym.* 87(1), 816-821.

[40] Aguilera, J. M. (2005). Why food microstructure? *J. Food Eng.* 67, 3–11.

[41] Brummell, D. A., Harpster, M. H. (2001). Cell wall metabolism in fruit softening and quality and its manipulation in transgenic plants. *Plant Mol. Biol.* 47, 311–340.

[42] Davies, L. M., Harris, P. J. (2003). Atomic force microscopy of microfibrils in primary cell walls. *Planta* 217, 283–289.

[43] Marga, F., Grandbois, M., Cosgrove, D. J., Baskin, T. I. (2005). Cell wall extension results in the coordinate separation of parallel microfibrils: Evidence from scanning electron microscopy and atomic force microscopy. *Plant J.* 43, 181–190.

[44] Cybulska, J., Zdunek, A., Psonka-Antonczyk, K. M., Stokke, B. T. (2013). The relation of apple texture with cell wall nanostructure studied using an atomic force microscope. *Carbohydr. Polym.* 92(1), 128-137.

[45] Barondes, S. H., Castronovo, V., Cooper, D. N., Cummings, R. D., Drickamer, K., Feizi, T., Gitt, M. A., Hirabayashi, J., Hughes, C., Kasai, K., et al. (1994). Galectins: a family of animal beta-galactoside-binding lectins. *Cell* 76, 597–598.

[46] Barondes, S. H., Cooper, D. N., Gitt, M. A., Leffler, H. (1994). Galectins-structure and function of a large family of animal lectins. *J. Biol. Chem.* 269, 20807–20810.

[47] Gunning, A. P., Pin, C., Morris, V. J. (2013). Galectin 3-β-galactobiose interactions. *Carbohydr. Polym.* 92, 529-533.

[48] Murray, P. J., Wynn, T. A. (2011). Protective and pathogenic functions of macrophage subsets. *Nat. Rev. Immunol.* 11, 723–737.

[49] Wells, C. M., Bhavsar, P. J., Evans, I. R., Vigorito, E., Turner, M., Tybulewicz, V., Ridley, A. J. (2005). Vav1 and Vav2 play different roles in macrophage migration and cytoskeletal organization. *Exp. Cell Res.* 310, 303–310.

[50] Bhavsar, P. J., Vigorito, E., Turner, M., Ridley, A. J. (2009). Vav GEFs regulate macrophage morphology and adhesion-induced Rac and Rho activation. *Exp. Cell Res.* 315, 3345–3358.

[51] Franz, C. M., Puech, P. H. (2008). Atomic force microscopy: a versatile tool for studying cell morphology, adhesion and mechanics. *Cell Mol. Bioeng.* 1, 289–300.

[52] Wang, J., Wan, Z., Liu, W., Li, L., Ren, L., Wang, X., Sun, P., Ren, L., Zhao, H., Tu, Q., Zhang, Z., Song, N., Zhang, L. (2009). Atomic force microscope study of tumor cell membranes following treatment with anti-cancer drugs. *Biosens. Bioelectron.* 25, 721–727.

[53] Bitler, A., Dover, R., Shai, Y. (2012). Fractal properties of macrophage membrane studied by AFM. *Micron* 43, 1239–1245.

[54] Duchene, D., Touchard, F., Peppas, N. A. (1988). Pharmaceutical and medical aspects of bioadhesive systems for drug administration. *Drug Dev. Ind. Pharm.* 14, 283–318.

[55] Sriamornsak, P., Wattanakorn, N., Takeuchi, H. (2010). Study on the mucoadhesion mechanism of pectin by atomic force microscopy and mucin-particle method. *Carbohydr. Polym.* 79, 54-59.

[56] Mitchison, T. J., Cramer, L. P. (1996). Actin-based cell motility and cell locomotion. *Cell* 84, 371–379.

[57] Zhang, P., Li, H. (2011). Direct Measurements of the Mechanical Stability of Zinc-Thiolate Bonds in Rubredoxin by Single-Molecule Atomic Force Microscopy. *Biophys. J.* 101(6), 1467–1473.